Bhabha Atomic Research Centre
Mumbai, India

National Facility for Neutron Beam Research

Editorial

National Facility for Neutron Beam Research (NFNBR) provides a variety of instruments for the scientific community. This facility is operated by Solid State Physics Division (SSPD), Bhabha Atomic Research Centre. Scientists from BARC, other DAE units, universities and national laboratories are welcome to use this facility through collaborative research projects. Many of these collaborations could be supported by UGC-DAE Consortium for Scientific Research, Board of Research in Nuclear Sciences (BRNS) and other agencies.

We sincerely thank everyone who contributed to this booklet.

Editors

Amit Kumar, Surendra Singh, Debasis Sen and Mala N Rao
Solid State Physics Division
Bhabha Atomic Research Centre, Mumbai – 400085.

January 2024

Contents

NFNBR

National Facility for Neutron Beam Research

Neutron scattering in the country started with the facility at Apsara reactor (1 MW) in 1956, and then continued with CIRUS (40 MW), which became available in 1960 and then with Dhruva, the present reactor. Dhruva is a 100 MW natural uranium reactor with peak thermal neutron flux of 1.8×10^{14} n cm^{-2} s^{-1}, tailor-made for neutron scattering experiments with tangential beam holes, through-tube, provision for separate moderators for cold and hot neutrons, guide-tube, etc. Advanced instruments, with fully automatic instrument control and data acquisition modes have been installed on various beam ports. State of the art technology was used to design and fabricate the spectrometers. 1-D and 2-D position sensitive detectors (PSD), and associated electronics have also been developed indigenously.

National Facility for Neutron Beam Research (NFNBR) has been created as a part of the Solid State Physics Division (SSPD) during early nineties to cater to the needs of the Indian scientific community in the field of neutron beam research. Scientists from BARC, other DAE units, universities and national laboratories use NFNBR through collaborative research projects. Many of these collaborations are being supported by UGC-DAE Consortium for Scientific Research, Board of Research in Nuclear Sciences (BRNS) and other agencies.

International collaboration between neutron beam research group at BARC and other countries is over six decades old. The first such agreement was the “Indian-Philippines-IAEA Agreement” signed during sixties, under which BARC-built neutron instrument was installed at Philippines, and their scientists were trained to use it. Another example is the installation of a neutron spectrometer at Bangladesh through IAEA. Scientists from Philippines, Korea, Indonesia, Bangladesh, Vietnam, Malaysia and Egypt have visited BARC to work on the neutron instruments. NFNBR installed a neutron instrument on the spallation neutron source at Rutherford Appleton Laboratory in UK. Scientists from SSPD avail advanced sources at UK, USA, Germany, France, Switzerland, Japan and other countries to carry out front line research, and keep themselves up to date in this field. The Institut Laue-Langevin, France and India have cooperated on technology transfer in various fields including the development of supermirror based polarizers.

Figure 1. A panoramic view of CIRUS and Dhruva reactors at BARC

General layout in the reactor hall and the guide tube laboratory is shown in Figure 2. There are four spectrometers at the tangential beam lines, two at the ends of the through tube, two at the radial beam lines looking at the hot source position, and four instruments in the guide tube laboratory.

The present-day facilities include single-crystal and powder diffractometers, polarized neutron spectrometer, High-Q diffractometer, triple-axis and time of flight spectrometers, quasi-elastic scattering spectrometer, all installed in the reactor hall, and two small-angle scattering instruments, reflectometer and detector test facility in the guide tube laboratory.

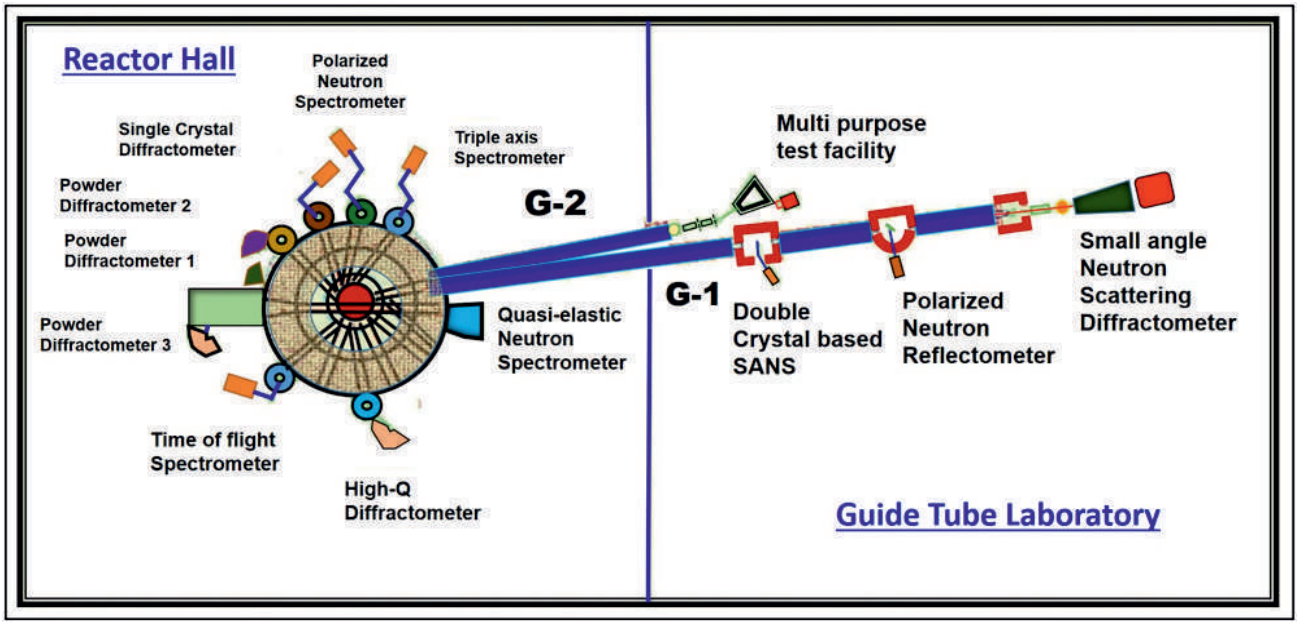

Figure 2. A layout of the neutron scattering instruments at Dhruva reactor

Figure 3. A view of neutron scattering facilities inside the Dhruva reactor hall

Neutrons for Condensed Matter Research

The existence of a neutral particle with mass similar to the mass of a proton, was hypothesized by Rutherford in 1920 and this was proved by the discovery of neutron by J. Chadwick, a student of Rutherford, in 1932. Since its discovery, neutrons are being used as an indispensable probe for research in condensed matter.

Due to its various special properties, neutrons provide an insight about the microscopic structures and dynamics in a wide class of materials. When scattered by materials, neutrons can not only help determine the position of an atom in that material but also atomic movement with time.

Properties of thermal neutron which make it an indispensable probe for research in condensed matter

- ❑ **Wave-particle duality**
- ❑ **Compatible wavelength** with the inter-atomic distances
- ❑ **Compatible energy** with the atomic excitation energy
- ❑ **Deep penetration** due to the charge neutrality
- ❑ Property to comprehend neighbouring Z elements due to significant difference in **scattering contrast**
- ❑ Isotope specific scattering and absorption
- ❑ Has **magnetic moment** (-1.913 nuclear magneton) and thus can interact with magnetic materials
- ❑ Interacts with nuclei in a simple way (isotropic s-wave scattering). No angular dependence of scattering amplitude for nuclear scattering unlike in the case of x-ray.

No Charge
Large penetration, probes bulk samples

Nuclear Scattering
Light elements, Differentiating isotopes, Neighbouring-Z elements

Magnetic Moment
Magnetic structure

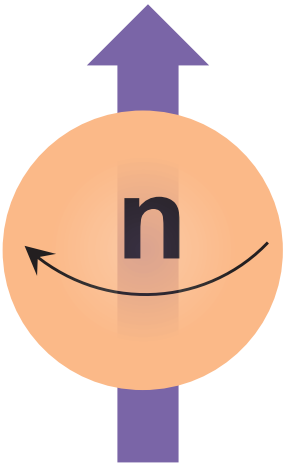

λ~ Interatomic distance
Crystal structure, Atomic position

Coherent/ Incoherent Scattering
Collective phenomena/ Single atom diffusion

Elementary excitations
Dynamic properties/Excitation energy

Particle nature

- Mass = 1.674 x 10^{-27} Kg
- Spin (1/2)
- Velocity [(2200m/s) for thermal neutrons with energy 25 meV]
- Acts as a tiny magnet

Wave nature

- Diffraction and interference pattern
- Measurable wavelength
- Measurable scattering length

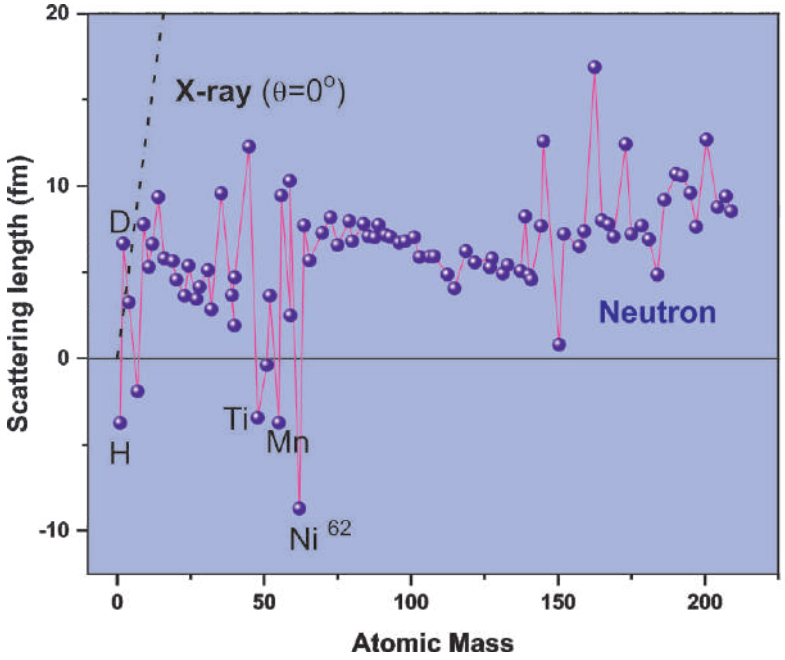

Element	Bound Coherent Scattering Length (fm)
H	-3.739
D	6.671
C	6.646
^{58}Ni	14.4
^{62}Ni	-8.7
Cu	7.718
Ti	-3.438
Fe	9.45

Unlike x-rays, the neutron scattering power of elements varies in a zigzag fashion with respect to the atomic mass. Due to this special property, neutron can differentiate neighbouring elements in a material and even sees distinctly the different isotopes of an element. Neutrons also allow to probe light atoms that are barely visible with x-rays. The scattering length of neutron for a few isotopes of some elements are negative. Hydrogen has a negative scattering length (-3.739 fm) while Deuterium possesses a positive scattering length (6.671 fm). Suitable combination of materials with positive and negative scattering length can be used to tune the neutron scattering contrast. Contrast matching experiments are used to obtain multi level structures.

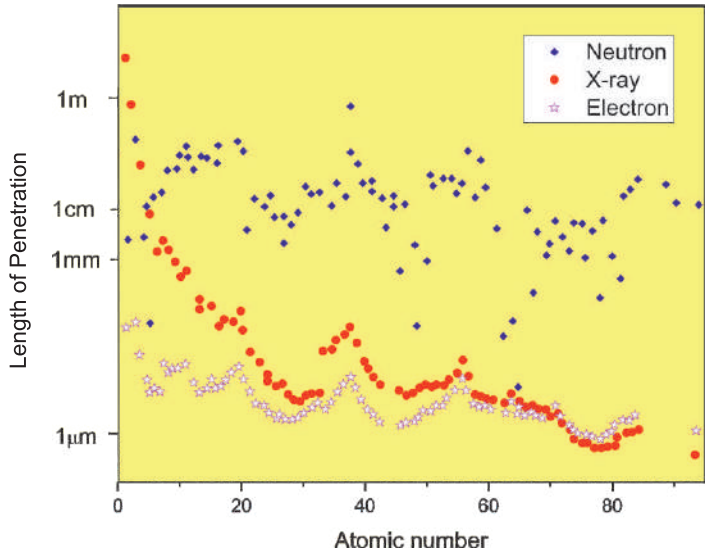

As the neutron does not carry any electric charge, the neutron has no electrostatic interaction with the electron cloud of an atom. For this reason, the neutron has a higher penetration power comparable to x-ray or electrons.

Neutron has spin ½ and is sensitive to the magnetic fields created by unpaired electrons. In magnetic materials, the order in magnetic structures and the interactions can be obtained using neutron scattering.

General References

1. G.E. Bacon, Neutron Diffraction (Clarendon Press, 1975).
2. P.A. Egelstaff (ed.) Thermal Neutron Scattering (Academic Press, 1965).
3. W. Marshall and S.W. Lovesey, Theory of Thermal Neutron Scattering (Clarendon Press, 1971).
4. G. L. Squires, Introduction to the Theory of Thermal Neutron Scattering (Cambridge University Press, 1978).
5. D. S. Sivia, Elementary Scattering Theory For X-ray and neutron users (OXFORD University Press, 2010).
6. A. Furrer, J. Mesot, T. Strässle, Neutron Scattering in Condensed Matter Physics (World Scientific, 2009).

Single crystal diffractometer

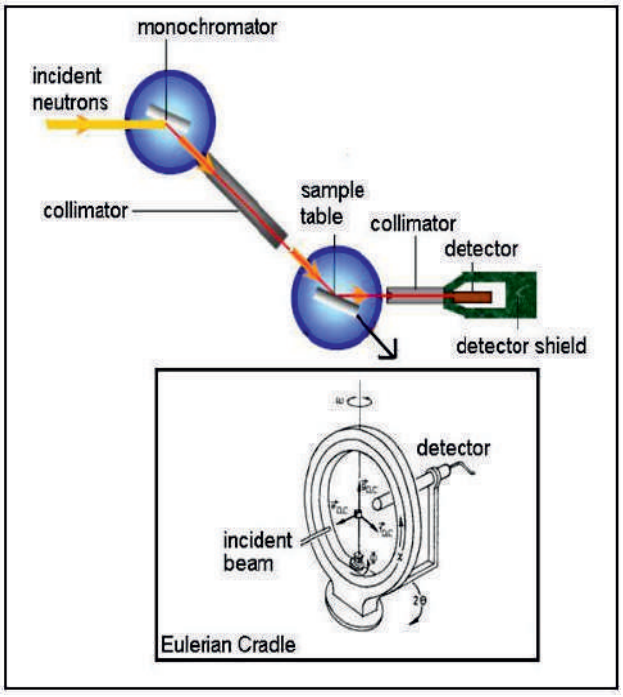

Instrument parameters

Beam port	T1011
Monochromator	Cu(220)
Wavelength	0.995 Å
Flux at sample	5×10^5 n/ cm^2/sec
Scattering angle	$0^\circ < 2\theta < 90^\circ$
Detector	BF_3 Counter

The four circle diffractometer is located at T1011 beam line of the Dhruva reactor. In a four circle diffractometer, the crystal is rotated about three Eulerian axes χ, ϕ and ω, and the detector is rotated about the 2θ axis. These four axes meet at a point, which is the centre of the diffractometer. The χ circle is mounted on the ω axis, while the ϕ circle is mounted on the χ-axis as shown in Figure. The crystal is mounted on the ϕ-axis. The geometry of axes mounting enables any reciprocal lattice point to be brought into the equatorial plane of the diffractometer.

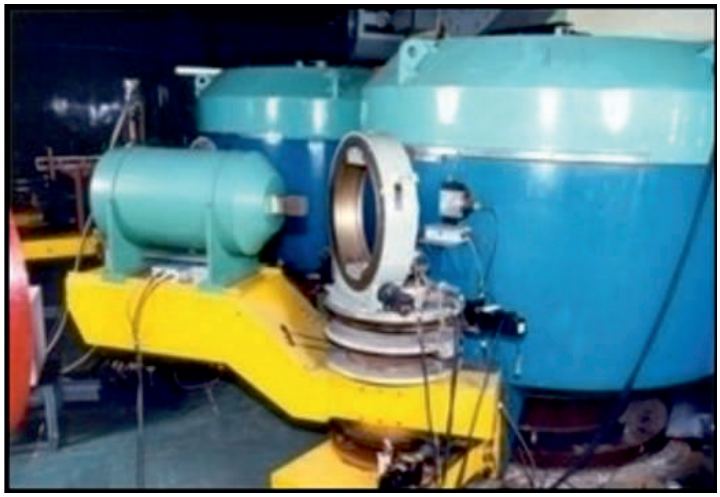

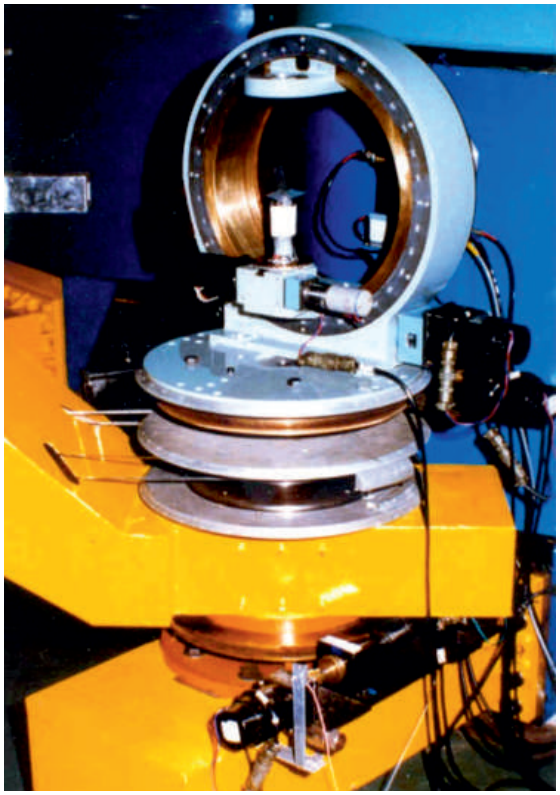

This instrument is used to study high precision three dimensional structure of materials, where hydrogen plays a major role in either the stereochemistry or the physical properties of the material. These include hydrates, biomolecules, ferro-electrics, electro optic material, super protonic conductors etc.

❑ Selected examples

❖ Deterioration of hydrogen bonded superprotonic conductors belonging to $CsHSO_4$–CsH_2PO_4–H_2O solid solution system: A single crystal neutron diffraction investigation

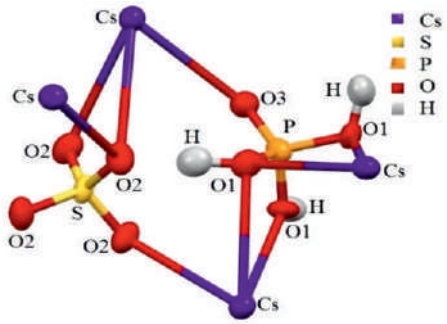

Asymmetric unit of $Cs_6H(HSO_4)_3(H_2PO_4)_4$

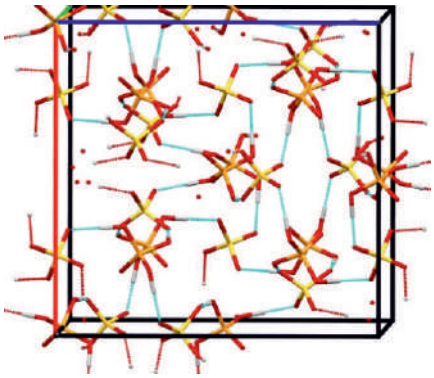

Hydrogen bonding network in $Cs_6H(HSO_4)_3(H_2PO_4)_4$

Single crystal neutron diffraction investigation on $Cs_4(HSO_4)_3(H_2PO_4)$ and $Cs_6H(HSO_4)_3(H_2PO_4)_4$ superprotonic crystals belonging to $CsHSO_4$–CsH_2PO_4–H_2O solid solution system was undertaken to elucidate the precise hydrogen atom positions in these crystals. The investigation revealed that these crystals are very sensitive to the ambient conditions and can undergo deterioration due to fluctuation in air moisture content. Crystal structure of $Cs_6H(HSO_4)_3(H_2PO_4)_4$ was obtained both before and after deterioration; it was found that the asymmetric O-H···O hydrogen bond between the PO_4 and SO_4 ions (Figure) of this crystal becomes stronger after deterioration, this led to the shrinkage of the unit cell, and most likely prevented further deterioration. The change in the hydrogen bonding is expected to affect the overall proton conductivity of the crystal.

Bull. Mater. Sci 44:108, (2021)

❖ L-Histidine with nitric acid: A comparison of Crystal structures and Hirshfeld surfaces analysis

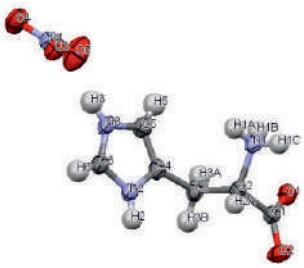

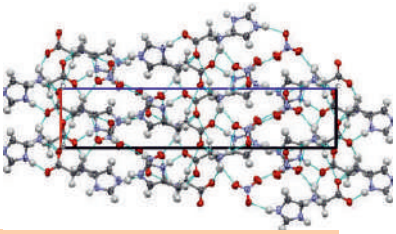

Asymmetric unit and packing in L-histidinium nitrate

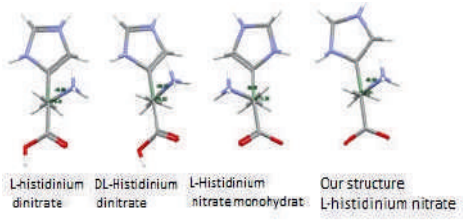

Conformation of L-histidine

L-Histidine and Nitric acid in water can give rise to three different crystals. L-histidinium nitrate, L-histidinium nitrate monohydrate, L-Histidinium dinitrate. In order to understand the hydrogen bonding interaction in L-histidinium nitrate, single crystal neutron diffraction was taken up. The crystal structure consists(Figure) one L-histidine molecule which has the amino and imino groups protonated, but the carboxylic acid group is deprotonated. The nitrate ion is in anionic state. A comparison of conformation and interatomic interaction was carried out in all the three structures. It was found that L-histidine in L-histidinium nitrate monohydrate adopts gauche (+) conformation and in other three structures it is gauche (-)(Figure). Interaction energy obtained from energy framework showed that L-histidine nitrate monohydrate has maximum total energy of -41.5(kJ/Mole). It was found that the average first hyperpolarizabilities of L-histidinium nitrate monohydrate was the highest amongst the three showing that it is more suitable for NLO material.

Journal of Molecular Structure,1267,133550 (2022)

❑ Selected Publications

1. R. Chitra, R.R. Choudhury, R.V. Rajan, D. Sajan, M. Kumar, Journal of Molecular Structure,1267,133550 (2022).
2. R R Choudhury, R. Chitra, I P Makarova, E V Selezneva and V A Komornikov Bull. Mater. Sci 44:108, (2021).
3. R R Choudhury, R. Chitra, Pramana - Journal of Physics 91(4),53, (2018).
4. E.V. Selezneva, I.P. Makarova, V V Grebenev, R. Chitra, R R Choudhury, Crystal. Reports,63(4), pp. 553-562, (2018).
5. R R Choudhury, R. Chitra, Bulletin of Materials Science 41(1),8, (2018).

Powder Diffractometer-1

Powder Diffractometer-1 is a high intensity and medium resolution, low temperature based neutron powder diffractometer installed at through-tube (beam port TT1015). This instrument is dedicated for the study of advanced functional magnetic materials.

Instrument parameters

Beam port	TT1015
Monochromator	Si (422)
Wavelength	1.094 Å
Resolution(Δd/d)	~1 %
Flux at sample	$5x10^5$ n/cm^2/s
Monochromator take-off angle ($2\theta_M$)	60°
Scattering angle	3° - 70°
Detector	Three linear position sensitive ^{3}He detectors (each 1-meter long)
Sample environment	Temperature range: 2.5 – 300 K

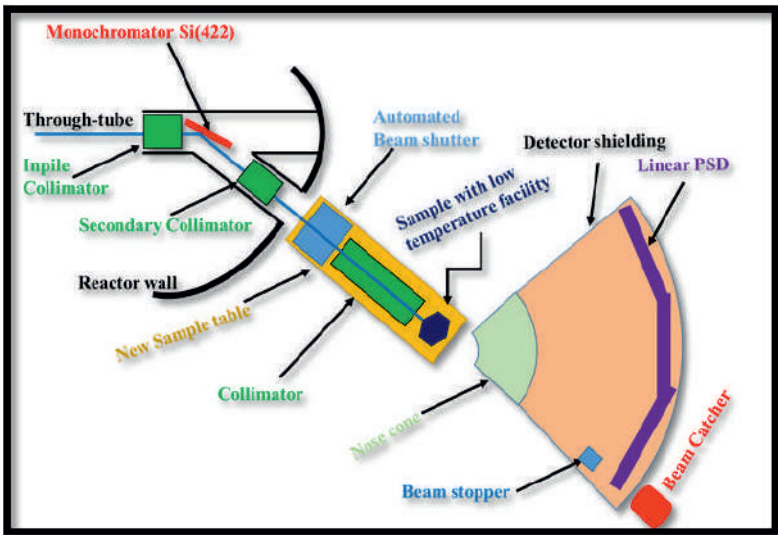

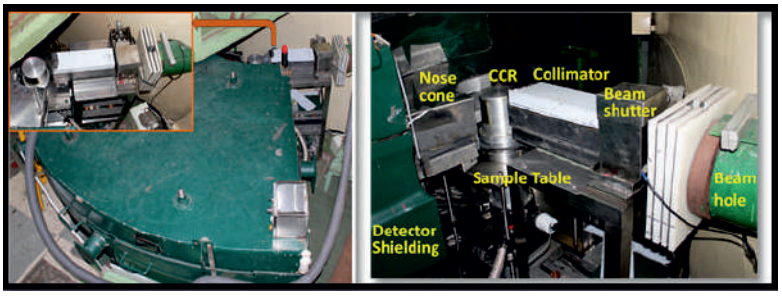

The diffractometer is extensively used for studying temperature dependent crystal and magnetic structural correlations in advanced magnetic materials including low-dimensional quantum magnets, multiferroics, molecular magnets, MOF magnets, perovskites, spinels, garnets etc. The software enabled automated data acquisition system allows recording of various sequences of measurements with respect to sample temperature and neutron flux.

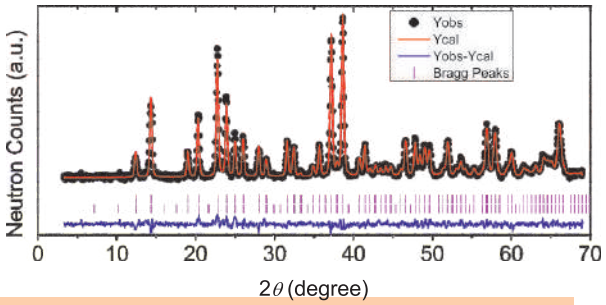

A representative neutron diffraction pattern (standard YIG sample) from PD-1

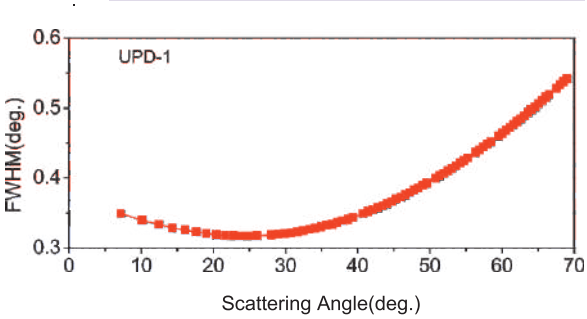

The resolution profile of PD-1

- S.K. Paranjpe and Y. D. Dande, Pramana-J. Phys. **32**, 793 (1989).
- S.K. Paranjpe and S. M. Yusuf, Neutron News **13,** 36 (2002).
- K. S. Chikara, A. K. Bera, A. Jain, A. Kumar, Upgradation of PD-1, SSPD Report, (2024).

❑ Selected examples

Neutron diffraction is a unique tool to study crystal and magnetic structures at the atomic level. Temperature dependent neutron diffraction measurements provide unique ways to study both structural and magnetic phase transitions as well as explore possible correlations between lattice, spin, and charge degrees of freedom.

❖ Spin-spin correlations in low-dimensional quantum magnets

Quantum magnets are in the forefront of current condensed matter physics research due to their unconventional properties, dictated by quantum fluctuations, including spin-liquid state, spin-nematic state, quantum phase transition, magnetization plateau states, and Bose-Einstein condensation state. Determination of the spin-spin correlations in these quantum magnets is the primary step towards the understanding of exotic properties. Powder Diffractometer-1 has been widely utilized to determine the spin–spin correlations in various quantum magnetic materials having long-range and/or short-range magnetic ordering.

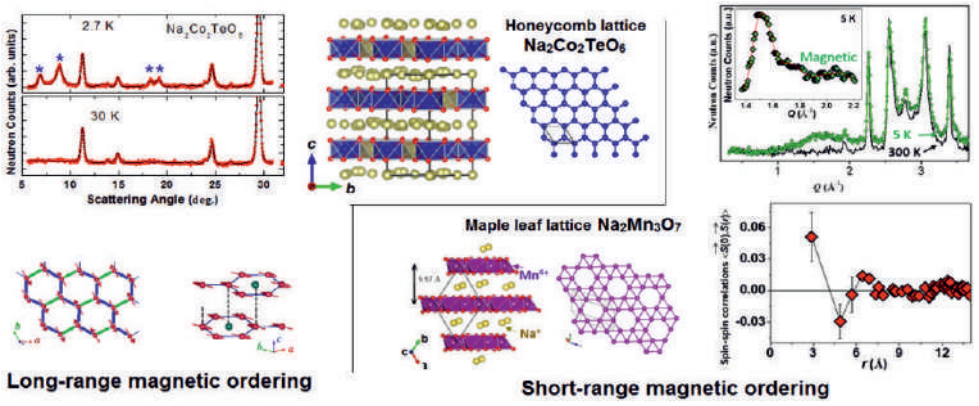

Appearance of magnetic Bragg peaks (marked with asterisks) in the neutron diffraction pattern at 2.7 K (top left) reveal the long-range magnetic ordering with zigzag AFM structure (bottom left) for the 2D honeycomb lattice compound $Na_2Co_2TeO_6$ (top middle). In contrast, the appearance of broad magnetic diffuse peak (top right) for 2D maple leaf lattice compound $Na_2Mn_3O_7$ (bottom middle) reveals the short-range magnetic ordering (bottom right).

Physical Review B 107 064419 (2023),
Physical Review Mater. 7, 085001 (2023)

❖ Structure-property correlations in multifunctional magnetic material

Multifunctional materials serve as the foundation for the next generation devices having improved energy efficiency and rapid responsiveness. For efficiency enhancement, it is crucial to understand the correlations between physical properties and the underlying crystal structure of the multifunctional materials. Neutron diffraction has been serving as an important experimental tool for investigating correlations of crystal structure with the electronic, magnetic, elastic and spintronic properties, allowing for the fine-tuning of physical properties by crystal engineering. Additionally, neutron diffraction has been used to illustrate the ionic conduction pathways in the unit cell, thus providing insights of the ionic conduction mechanisms in highly efficient battery materials.

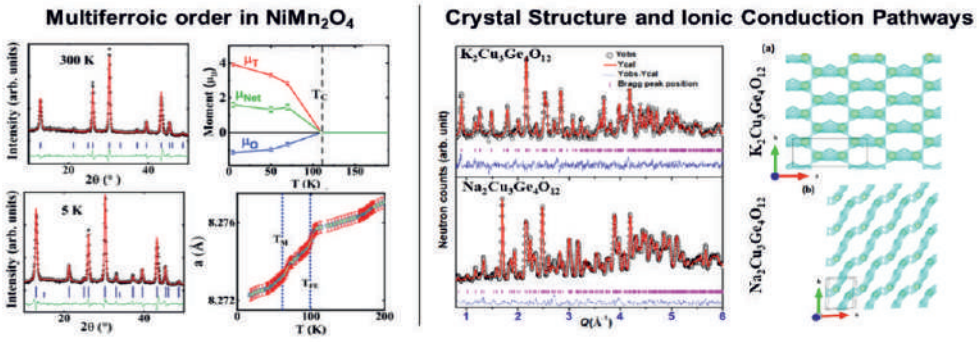

(left) The magnetoelastic coupling has been demonstrated by the anomaly in the lattice parameter at magnetic ordering temperature Tc in $NiMn_2O_4$ by temperature dependent neutron diffraction study using PD-1. (right) The microscopically different ionic conduction pathways in isoformula compounds $K_2Cu_3Ge_4O_{12}$ and $Na_2Cu_3Ge_4O_{12}$ have been illustrated by the soft-Bond Valence analysis of neutron diffraction patterns measured at PD-1.

J. Appl. Phys. 134, 104103 (2023),
ACS Appl. Electronics materials 5, 2704 (2023)

❑ Selected Publications

1. B. Saha, A. K. Bera, S. M. Yusuf, and A. Hoser, Physical Review B 107 064419 (2023).
2. B. Saha, A. K. Bera, S. Kesari, and S. M. Yusuf , Physical Review Mater. 7, 085001 (2023).
3. Deepak, A. Kumar, A. K. Bera, and S. M. Yusuf, Physical Review Mater. 6, 074405 (2022).
4. Deepak, A. Kumar, and S. M. Yusuf, Physical Review Mater. 5, 124402 (2021).
5. Sebin J. Sebastian, S. S. Islam, A. Jain, S. M. Yusuf, M. Uhlarz, and R. Nath, Physical Review B 105, 104425 (2022).

Powder Diffractometer-2

This is a conventional neutron diffractometer and caters mainly to understand long range order in polycrystalline materials.

Instrument parameters

Beam port	T1013
Monochromator	Ge(331)
Wavelength	1.2443 Å
($\Delta d/d$)	~0.8 %
Flux at sample	8.5×10^5 n/cm^2/sec
Scattering Angle	$4^o < 2\theta < 140^o$
Q range	0.4 – 9.4 Å^{-1}
Beam Size	4.0 cm × 1.5 cm
Detector	5 (1-D) ^{3}He PSD
Sample Environment	(i) T =2K – 1400K (ii) B = upto 7 T (iii) P = upto 2 GPa

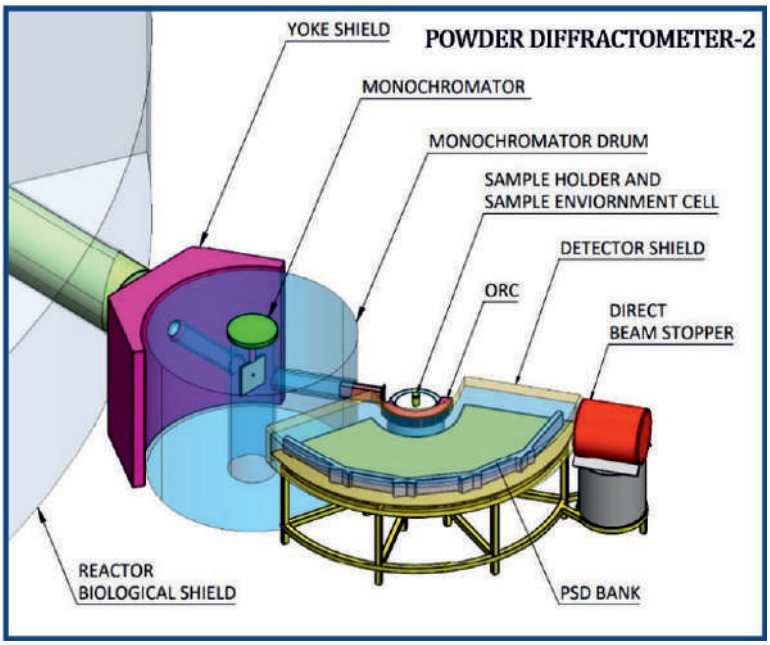

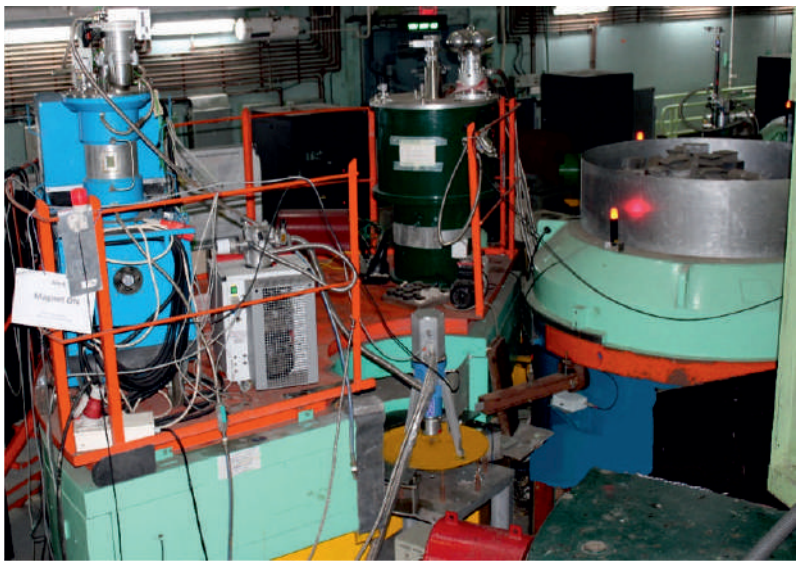

Powder diffractometer-2 is a multi-PSD based instrument covering Q-range up to 9.4 Å^{-1}. This instrument is being extensively used to study structural and magnetic transitions in alloys and compounds. It has been used for structural studies of a number of Ferro-electric materials, CMR materials, High T_c materials, SOFC materials, Low dimensional magnetic materials, Molecular magnetic materials and also in studies of local structure determination from ion conducting crystalline systems.

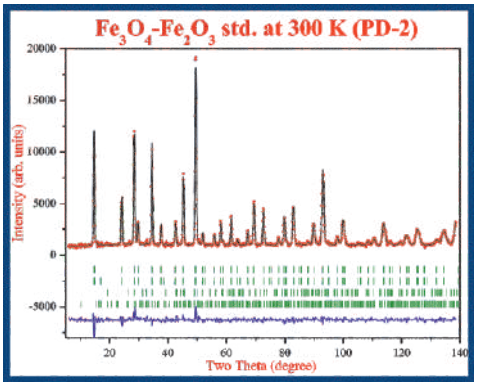

P.S.R.Krishna, A.B.Shinde, A.Das, S.S.Naik, S.K.Paranjpe and M. Ramanadham, Solid State Physics (India) 45 ,149 (2002).

❑ Selected examples

❖ Role of correlated disorder on structural stability and functional properties in (1-x)$NaNbO_3$-x($Ba_{0.7}Ca_{0.3}$)TiO_3

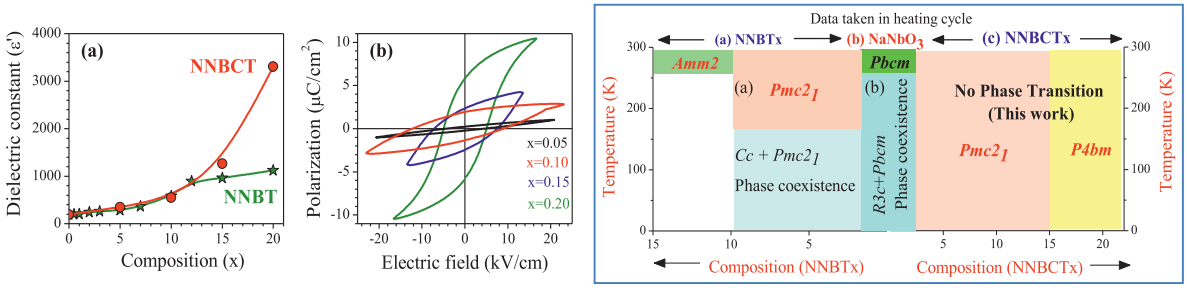

In perovskites, correlated disorder arises due to chemical substitution and stimulates the functional properties of these materials. Powder neutron diffraction measurements have been used in conjunction with electrical measurements to investigate the effect of correlated disorder in (1-x)$NaNbO_3$-(x)$BaTiO_3$ (NNBTx) solid solution by partially substituting the Ba site with Ca. The effect of correlated disorder on competition and cooperation between polar and antiferrodistortive mode has been investigated. Enhanced dielectric constant (by three times) is observed compared to NNBTx. Emergence/vanishing of diffraction peaks along with change in the intensities are observed in powder neutron diffraction data of (1-x)$NaNbO_3$-x($Ba_{0.7}Ca_{0.3}$)TiO_3 (NNBCTx). Analysis of this data suggests existence of a structural phase transition with composition change (x), while the phase stability of functional ferroelectric phase at room temperature is extended to lower temperatures. It has also been found that there is a gradual weakening of antiferrodistortive mode (R_4^+) and presence of spontaneous lattice strain. The structural parameters of low-temperature orthorhombic phase of NNBCT05 are modeled in the framework of Grüneisen approximation with a Debye approximation for the internal energy.

Journal of Alloys and Compounds 866, 158982, (2021)

❖ Origin of magnetic ordering in half-Heusler RuMnGa

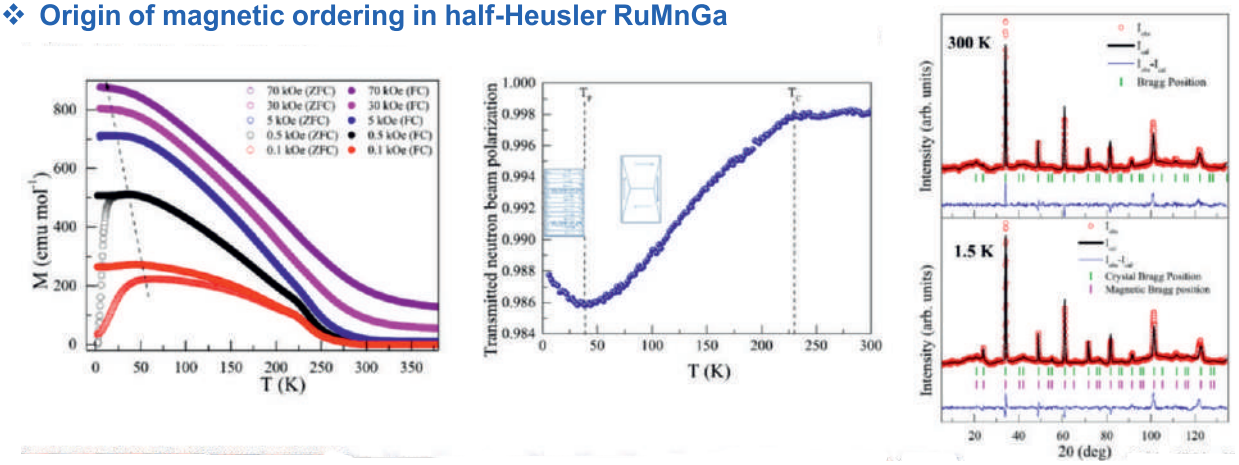

The half-Heusler alloy RuMnGa having valence electron count (VEC) 18 has recently been theoretically proposed to exhibit compensated ferrimagnetic (CFiM) character instead of the expected nonmagnetic ground state. The crystal structural and magnetic properties of RuMnGa have been investigated using x-ray/neutron diffraction, ac and dc magnetometry and neutron depolarization. We have shown that the system exhibits FM-type ordering owing to the inherent presence of this minor off-stoichiometry, showing very low magnetic moment. The system also exhibits reentrant canonical spin-glass behavior, which is rarely observed in half-Heusler alloys.

Phys. Rev. B 108, 054430 (2023)

❑ Selected Publications

1. Sourabh Wajhal, S.K. Mishra, A.B. Shinde, P.S.R. Krishna, R. Mittal, Journal of Alloys and Compounds 866, 158982 (2021).
2. V. B. Jayakrishnan, S. K. Mishra, A.B. Shinde, S. Wajhal, P.S.R. Krishna and P.U. Sastry, J. Solid State Chem. 322,123996 (2023).
3. PSR Krishna, SK Mishra, AB Shinde and Sourabh Wajhal, IANCAS Bulletin, Vol. XVIII, 6-16 (2022).
4. Madhu Ghanathe, A K Bera, Amit Kumar, and S. M. Yusuf, ACS Applied Electronic Materials 4, 394–405 (2022).
5. Deepak, Amit Kumar, SM Yusuf, Physical Review Materials 5, 124402 (2021).

Powder Diffractometer-3

This Diffractometer, with a doubly bent focusing monochromator, uses open-beam geometry for higher flux and enables use of small samples. A variety of chemical and magnetic structures of novel materials have been studied using the low temperature-high magnetic field sample environment.

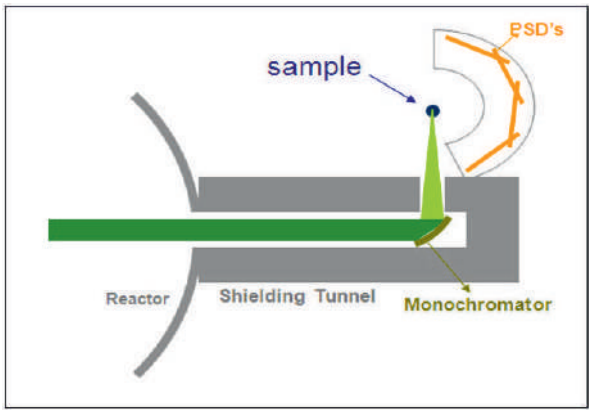

Instrument parameters

Beam port	TT-1015
Monochromator	Bent Si
Wavelength	1.17 Å, 1.48 Å (std), 1.76 Å, 2.31 Å
Beam size	15 x 25 mm^2
Flux at sample	7 x 10^7 $n.cm^{-2}s^{-1}$
Scattering angle	6 - 123^0
Q range	0.4 - 7.4 $Å^{-1}$
Δd/d	< 0.3 %
Detector	12 linear ^{3}He PSDs

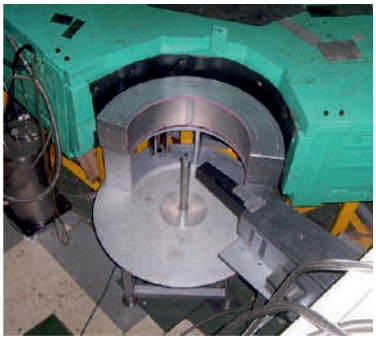

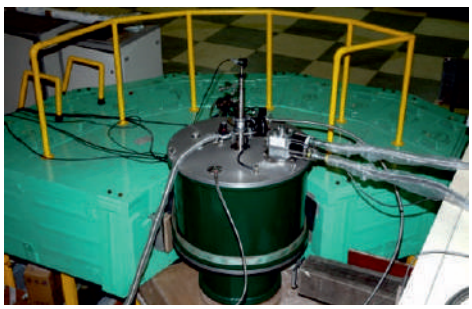

This powder diffractometer, developed and installed by UGC-DAE Consortium for Scientific Research, is a multi-PSD high throughput diffractometer.

It employs a bent perfect crystal monochromator at a take-off angle of 90 degrees and it is designed for a highly focused neutron beam of about 15x25 mm^2 in size. This enables higher flux at sample position and also use of small sample (~ 1 cc in volume). A complete diffraction pattern is obtained over four overlapping banks of three linear PSDs each, covering an angular range up to 123^0. The resolution obtained (Δd/d) is <0.3%

A. V. Pimpale, B. A. Dasannacharya, V. Siruguri, P. D. Babu and P. S. Goyal, Nucl. Instru. Meth, A481 (2002) 615.
V. Siruguri, P. D. Babu, M. Gupta, A. V. Pimpale, and P. S. Goyal, Pramana – J. Phys. 71 (2008) 1197.

❑ Selected examples

❖ Fluorination induced asymmetry in vacancy ordered brownmillerite: Route to multiferroic behavior

In multiferroics, ferroelectricity is driven by electronic lone pairs, geometry, charge ordering, and magnetism; with each having its limitation for technological applications.

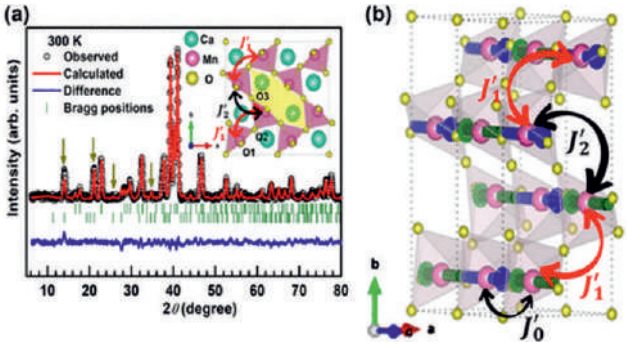

ND study of $Ca_2Mn_2O_5$ at RT signifying crystal and magnetic structure

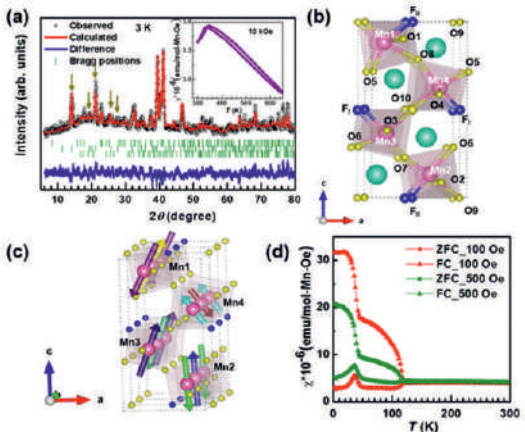

ND of Fluorinated $Ca_2Mn_2O_5$ at 3 K ascertains F position and exhibits spin orientation

A mechanism to achieve multiferroicity in a single phase by engineering anionic network and creating local geometric distortions in fluorinated, vacancy-ordered brownmillerite $Ca_2Mn_2O_{5-x}F_y$ is proposed in this study. Fluorinated system characterized by various techniques exhibits both ferroelectricity and an antiferromagnetic order above room temperature. Neutron diffraction played a pivotal role in ascertaining fluorine position at oxygen site.

Chem. Mater 35, 991 (2023)

❖ Incommensurate conical magnetic structure in $BaFe_{10}In_2O_{19}$

Temperature dependent neutron diffraction at 2.31 Å along with other characterization on $BaFe_{10}In_2O_{19}$ unequivocally point out towards presence of cluster-spin glass state below T_{SRT} which coexists with the long range incommensurate longitudinal conical magnetic structure.

Variation in the magnetic structure could clearly be ascertained through the analysis of data.

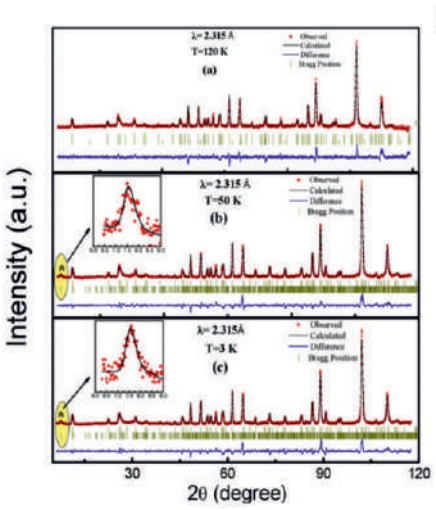

J. Alloys Compd. 825 154141 (2020)

Temp dependent appearance of magnetic peak.

Variation in spin orientation

❑ Selected Publications

1. S. Gupta, S. Mukherjee, P. D. Babu, S. D. Kaushik, K G Suresh et. al., J. Magn. Magn Mater 583, 170992 (2023).
2. R Harikrishnan, J. K. Bidika, A. J Chelvane, S. D. Kaushik, P. D. Babu, et. al. Phys Rev B, 108, 094407 (2023).
3. R. A. Saha, J. Sannigrahi, S. D. Kaushik, C. Meneghini, V. Siruguri, S. Ray, et. al. Phys. Rev. B, 107, 155105 (2023).
4. N Kumar, S. D. Kaushik, K Sandeep Rao, P D Babu, S K Deshpande, S N Achary, et. al. Crystals 13, 503 (2023).
5. P. Aich, C. Meneghini, V. Siruguri, S. D. Kaushik, T. S. Dasgupta, S. Ray et. al., Chem. of Mater, 35 991 (2023).

Polarized Neutron Spectrometer

Study of magnetic correlations

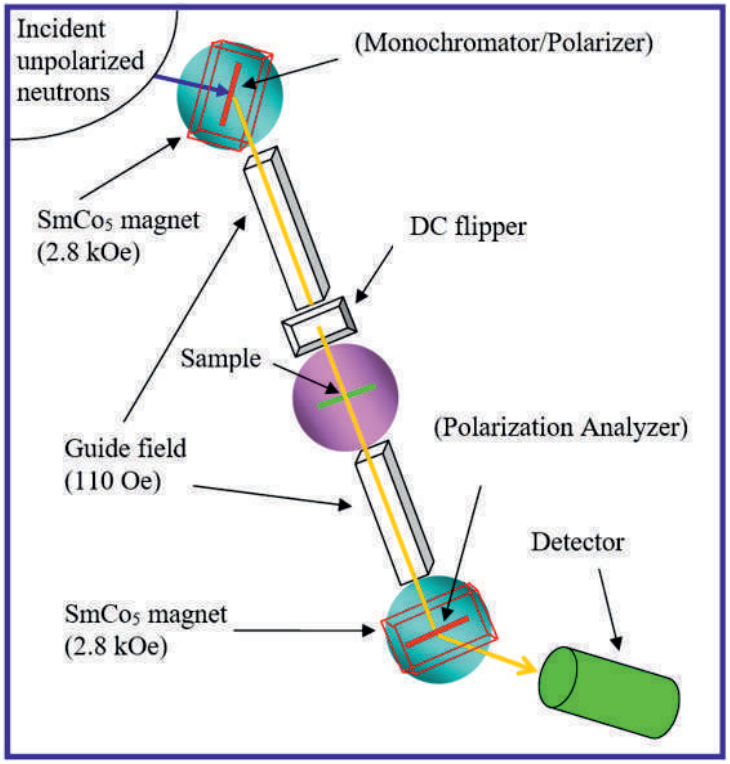

The polarized neutron spectrometer (PNS) is used for magnetic scattering studies. This spectrometer can be used in three different modes: (a) diffraction mode (2-axis configuration) (b) polarization analysis mode (3-axis configuration in scattering geometry), and (c) depolarization mode (3-axis configuration in transmission geometry). The instrument has been extensively used for studying magnetic properties of ferrites, 3d element based alloys, 3d-4f element based intermetallic compounds, amorphous magnets, CMR perovskites, and quasi 1-D chain magnets. Recently, it has been extensively used to study magnetization reversal phenomenon in spinels, garnets, intermetallic compounds, perovskites, and molecular magnets.

Instrument parameters

Beam port	T1009
Monochromator/ Polarizer	Cu_2MnAl (111)
Wavelength	1.201 Å
Beam Polarization	~98.83 %
Flux at sample	3.6×10^5 n/cm^2/sec
Analyzer	$Co_{0.92}Fe_{0.08}$ (200)
Scattering angle	2 - 90˚
Sample environment	*T* : 1.5 – 400 K *H* : ± 1.2 kOe *E* : ± 100 KV/cm
Detector	BF_3

S. M. Yusuf and L Madhav Rao, Neutron News 8, 12 (1997).
S. M. Yusuf and L Madhav Rao, Pramana- J. Phys. 47, 171 (1996).

❑ Selected examples

❖ Intertwined negative magnetization and exchange-bias in $DyFe_5Al_7$

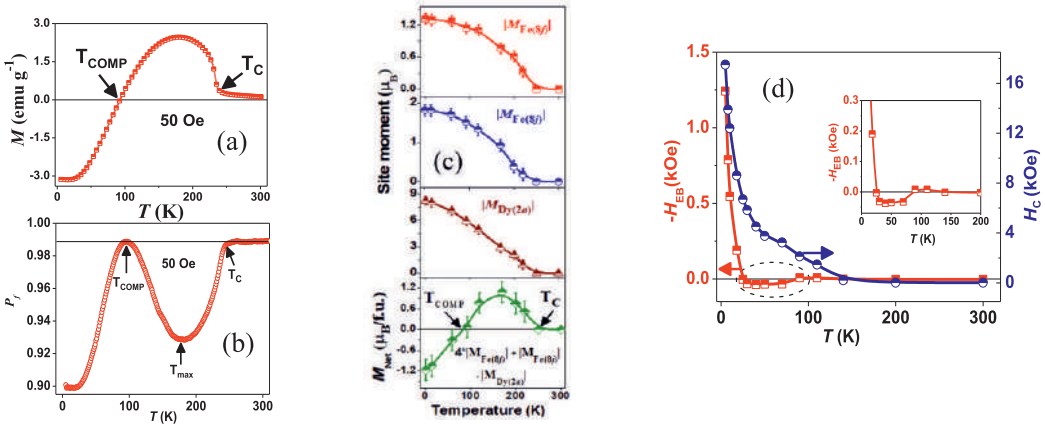

Coexistence of technologically important phenomena of negative magnetization [Fig. (a)] and exchange-bias has been probed in $DyFe_5Al_7$ compound by employing neutron diffraction and neutron depolarization techniques. A full compensation of magnetization of randomly oriented magnetic domains (at the T_{COMP}) in the sample is clearly demonstrated by neutron depolarization [Fig. (b)]. Neutron diffraction study has revealed the asymmetric thermal variations of ferrimagnetically coupled Dy and total Fe magnetic moments leading to a sign change of net magnetic moment at the T_{COMP} [Fig. (c)]. The reported exchange-bias [Fig. (d)] below the T_{COMP} shows an anomalous behaviour due the presence of field-induced spin reorientation in this intermetallic compound.

J. Phys.: Condens. Matter 35 065802 (2023)

❖ Role of Ho ordering in magnetization compensation in $Ho_3Fe_5O_{12}$

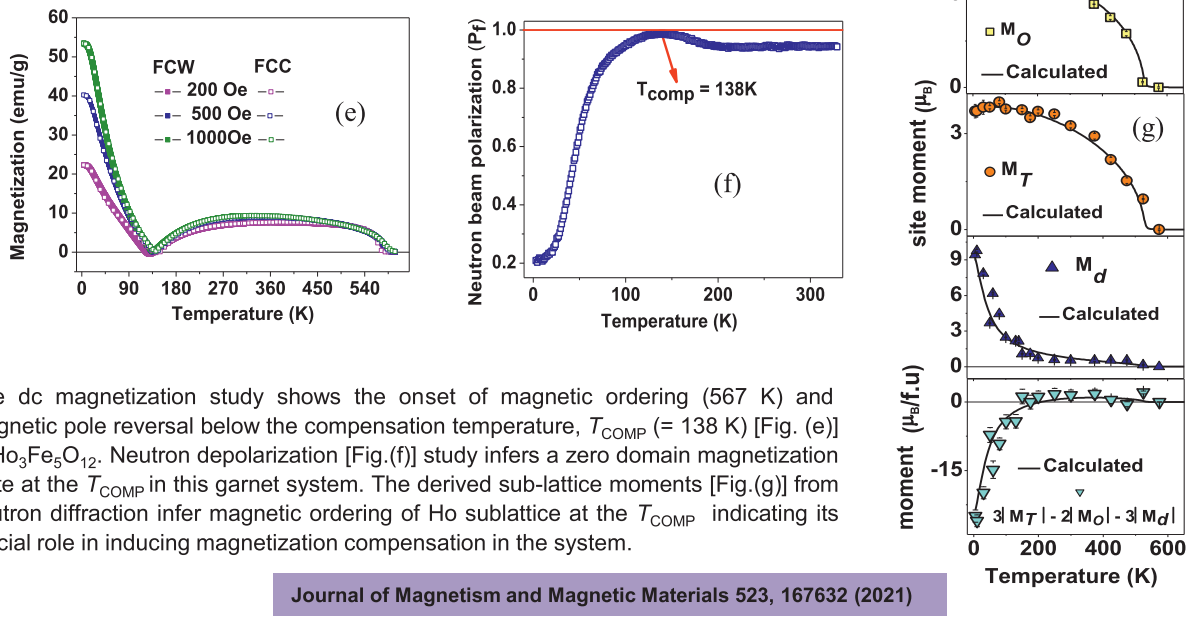

The dc magnetization study shows the onset of magnetic ordering (567 K) and magnetic pole reversal below the compensation temperature, T_{COMP} (= 138 K) [Fig. (e)] in $Ho_3Fe_5O_{12}$. Neutron depolarization [Fig.(f)] study infers a zero domain magnetization state at the T_{COMP} in this garnet system. The derived sub-lattice moments [Fig.(g)] from neutron diffraction infer magnetic ordering of Ho sublattice at the T_{COMP} indicating its crucial role in inducing magnetization compensation in the system.

Journal of Magnetism and Magnetic Materials 523, 167632 (2021)

❑ Selected Publications

1. A Chatterjee, A Kumar, PK Manna, S Bedanta, A Sarma, S Majumdar, SM Yusuf, S Giri, J. Appl. Phys. 134, 104103 (2023).
2. Deepak, A Kumar, AK Bera, SM Yusuf, Phys. Rev. Mater. 6, 074405 (2022).
3. Deepak, A Kumar, SM Yusuf, Phys. Rev. Mater. 5, 124402 (2022).
4. A Kumar, SK Giri, TK Nath, C Ritter, SM Yusuf, J. Appl. Phys. 128, 203901 (2020).
5. M Ghanathe, A Kumar, SM Yusuf, J. Appl. Phys. 125, 093903 (2019).

High-Q Diffractometer

This High-Q diffractometer is a conventional neutron diffractometer with high Q_{max} upto 17.6 $Å^{-1}$ and caters mainly to understand short range order in glasses, liquids and

Instrument parameters

Beam port	HS1019
Monochromators	V.F. Cu(220);λ = 0.783 Å Cu(002); λ = 1.107 Å Cu(111); λ = 1.278 Å Cu(113); λ = 0.667 Å
In-pile Collimations	5 ', 10 ', 20 ', Open
(ΔQ/Q) (%)	0.73, 1.07, 1.22, 1.60
Flux at sample n/cm²/sec	2.0×10^6 Cu(111) 4.4×10^6 Cu(002) 1.5×10^5 Cu(113) 1.0×10^6 Cu(220)
Scattering Angle	$4^o < 2\theta < 140^o$
Q_{max} value	9.2 $Å^{-1}$ - Cu(111) 10.6 $Å^{-1}$ - Cu(002) 17.6 $Å^{-1}$ - Cu(113) 15.0 $Å^{-1}$ - Cu(220)
Beam Size	4.0 cm × 1.5 cm
Detector	15 (1-D) ^{3}He PSD
Sample Environments	(i) 2K – 1400K (ii) P = upto 2 GPa

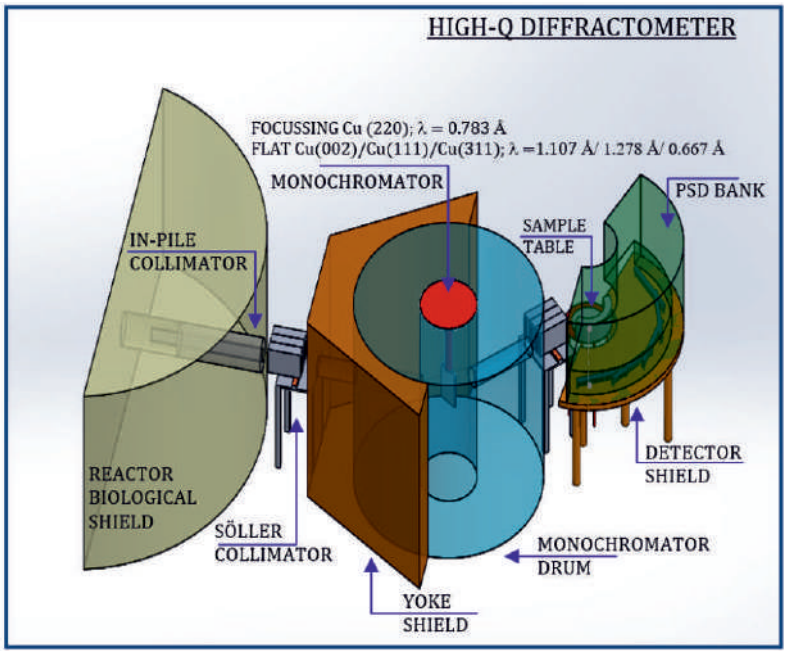

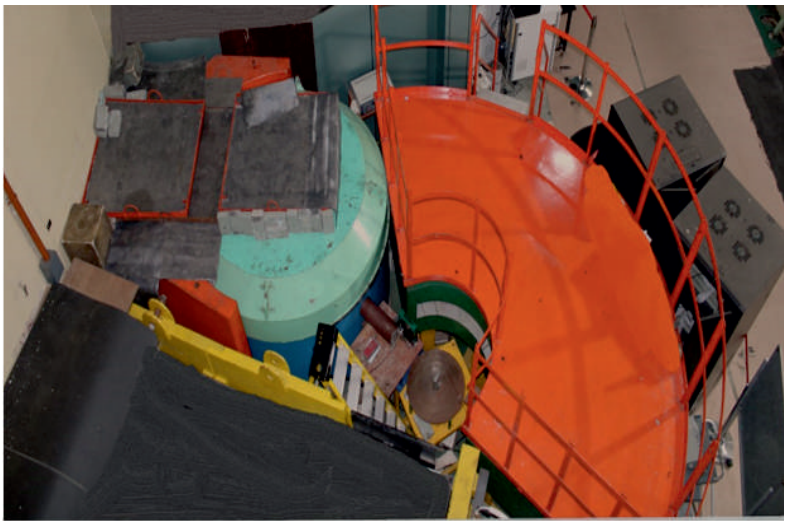

High-Q diffractometer has been upgraded and now it comprises of multiple intensity and resolution options along with the choice of four wavelengths. It can be used for structural studies of a number of Molecular fluids, Chalcogenide glasses, Borate glasses, Phosphate glasses, Tellurite glasses, Silicate glasses, different types of Carbon and also in studies of local structure determination from disordered crystalline systems. Experiments with smaller time frames, isotopic substitution of elements to acquire partial structure factors are possible. For polycrystalline materials, high-pressure experiments up to 2 GPa, Time-resolved diffraction and Pair Distribution Function analysis to study local structure are feasible.

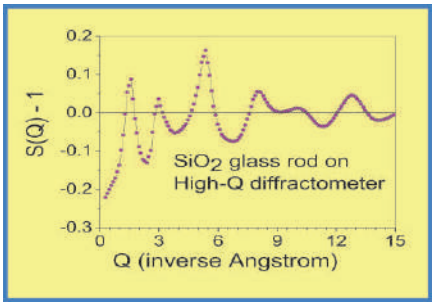

P.S.R. Krishna and A.B. Shinde, Solid State Physics (India), 45, 121 (2002).
B.A. Dasannacharya, P.S.R. Krishna and R. Chakravarthy Phys. B 180, 880 (1992).

❑ Selected examples

❖ Structure of Lanthanum-Tellurite Glass-Ceramics: A neutron diffraction study

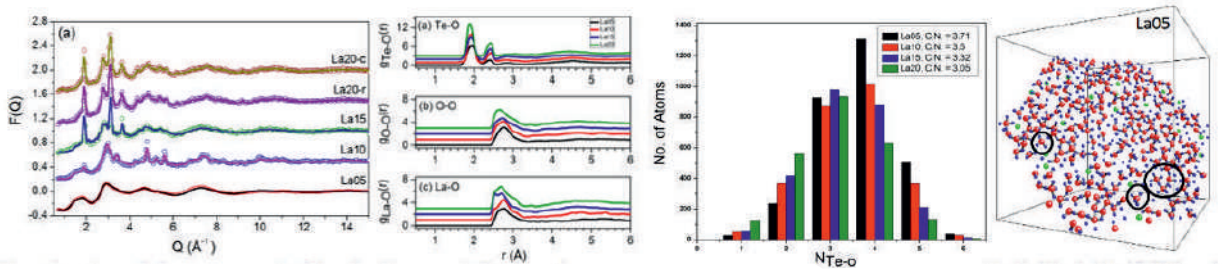

Structural models are reported for lanthanum tellurite glass-ceramics, $(La_2O_3)_x$ - $(TeO_2)_{1-x}$(x = 0.05, 0.10, 0.15, 0.20) using total neutron diffraction measurements. Reverse Monte Carlo modeling of total diffraction data has been used to build 3D configurations for these systems. The short range order and co-ordination number distribution has been successfully determined. The local structure is predominantly made up of TeO_4 trigonal bi-pyramid, TeO_3 trigonal pyramid, TeO_{3+1} and LaO_6 octahedra. The network connectivity x=0.05 to 0.15, is primarily based on connected TeO_4 and TeO_3 units via bridging oxygen atoms and in turn connected to La^{3+} via non bridging oxygen atoms. As La content increases more and more TeO_4 units get converted in to TeO_3 units. The number of TeO_3 structural units increases, thus decreasing the average Te co-ordination number, for glass-ceramics of higher La_2O_3 concentration. We observed that the local structure of the glasses has good resemblance to the short range order of corresponding crystalline phase and the network connectivity in the glasses can be linked to that of the distorted crystalline structure

IANCAS Bulletin Vol. XIX, 44-58,(2023)

❖ Structure of $xMoO_3$ -(1-x)TeO_2 glasses by neutron diffraction and Reverse Monte Carlo modeling

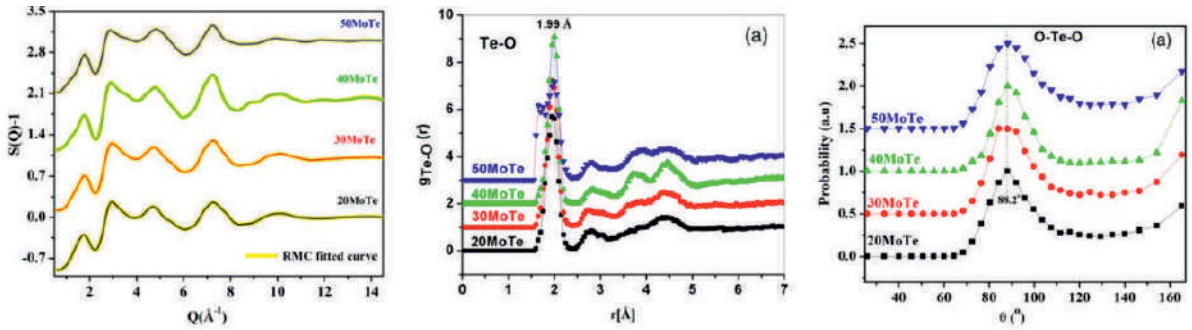

Short-range structural properties of glasses of the system: $xMoO_3$-(1-x)TeO_2 (x = 20, 30, 40 and 50 mol%) were studied by neutron diffraction. The diffraction data was modeled by Reverse Monte Carlo (RMC) simulations and the partial pair correlation distributions, Te–O, Mo–O, O–O bond-lengths/distances, Te and Mo speciation and the bond angle distributions were determined. It was found that TeO_3 , TeO_4 and TeO_5 are the major structural units and Mo ions exist in triangular, tetra, penta and hexa-units with the dominant fraction being that of MoO_4 and MoO_5 units in the glass network. Both the Te–O and Mo–O atomic pair distributions show peaks at same distances in the range: 1.97 ± 0.02 Å to 2.00 ± 0.03 Å and the Mo–O and Te–O structural units are found to have very similar dimensions and geometry. The O–Te–O and O–Mo–O bond angle distributions have peaks at 88.2°, which confirm that O eq-Te–O ax are the most abundant Te–O linkages in the glass network. The glasses do not show any systematic variation in the average Te–O and Mo–O co-ordinations on increasing MoO_3 concentration from 20 to 50 mol%, due to the dual character of MoO_3 as a network modifier and former.

Mater. Res. Express 6, 075211 (2019)

❑ Selected Publications

1. PSR Krishna, SK Mishra, AB Shinde and Sourabh Wajhal, IANCAS Bulletin Vol.XIX No.1, 44-58,[2023];AIP Conference Proceedings 2265, 030242 (2020).
2. Atul Khanna, Amandeep Kaur, Margit Fabian, P S R Krishna and A B Shinde, Mater. Res. Express 6, 075211 (2019).
3. Ranjan Mittal, et. al, Phys. Rev. B 102, 064103, [2020]; Phys. Rev. B 105, 104106 (2022).
4. Manjunath T. Nayak , J. A. Erwin Desa, P.S.R. Krishna, A.B. Shinde, et. al. Silicon, 14, 10337 (2022).
5. A Kaur, A Khanna, P. S. R. Krishna, A. B. Shinde, et. al., Phys. Chem. Glasses: Eur. J. Glass Sci. Technol. B, 61, 27–39 (2020).

Small-Angle Neutron Scattering Diffractometer

This is conventional slit-geometry SANS diffractometer. It makes use of a neutron velocity selector which can provide a monochromatic neutron beam of variable wave-length and wave-length resolution.

The monochromatic neutron beam passes through two slits before it is incident on sample. The sample position is equipped with an automated sample changer having slots to place seven samples. The angular distribution of the scattered neutrons is measured using 4 linear ^{3}He detectors, positioned in crisscross geometry.

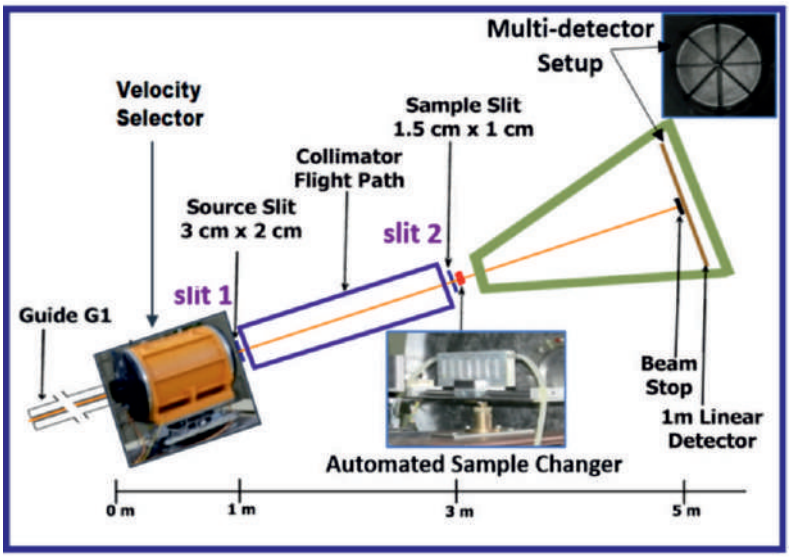

SANS-I Facility at BARC

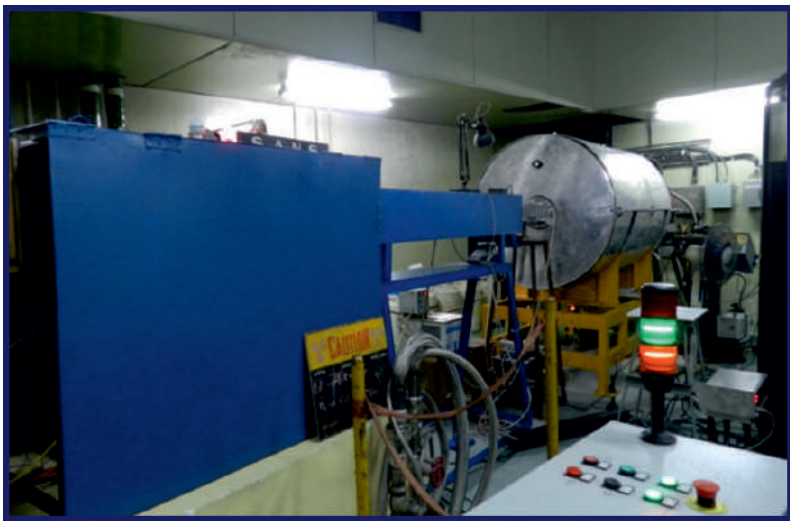

V. K. Aswal and P. S. Goyal, Curr. Sci. 79, 947 (2000).

Instrument parameters

Beam port	Guide G1
Monochromator	Velocity Selector
Wavelength	4 - 10 Å
$(\Delta\lambda/\lambda)$	10 - 20 %
Flux at sample	2 x 10^5 n/ cm^2/sec
Source slit (S1)	3 cm × 2 cm
Sample slit (S2)	1.5 cm × 1 cm
Distance S1 & S2	2 m
Distance S2 & D	2 m
Angular divergence	± 0.5^o
Detector	4 linear ^{3}He-PSDs
Q range	0.01 - 0.35 Å^{-1}
Temperature	20 - 80 ^{o}C

This facility is widely used to characterize different kinds of soft-materials, biomaterials and nanomaterials for their structure (shape, size, size-distribution) and interactions (attraction/repulsion, aggregation, ordering etc.). These systems typically consist of protein solutions, nanoparticle dispersions, amphiphiles, magnetic fluids, nano-bio complexes, polymers, gels, porous membranes and other colloidal dispersions.

Typical SANS Data

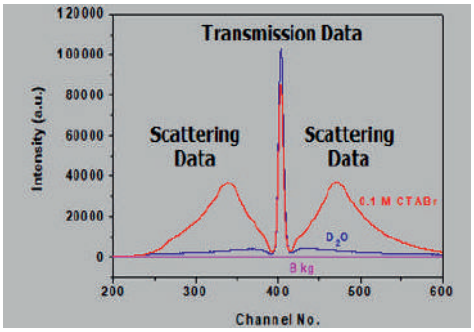

❑ Selected examples

❖ Tuning Heat-Induced Protein Gelation by Controlling Inter-Protein Interactions

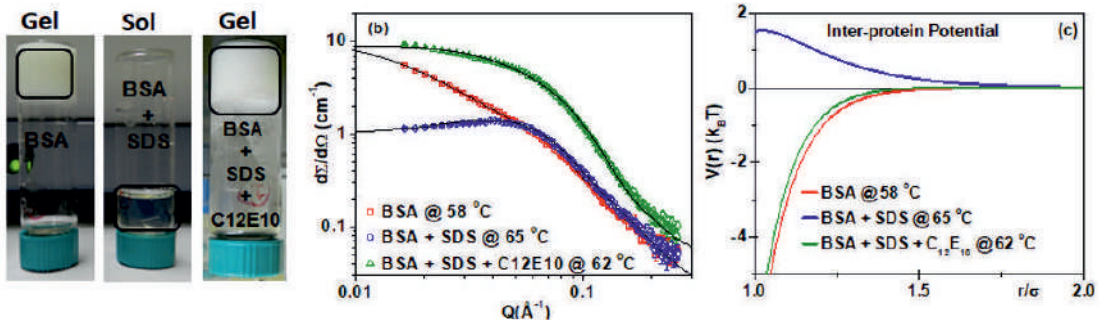

This work explores the pathways to control the temperature driven protein gelation by manipulating the electrostatic and hydrophobic interactions, having applications in a wide range of fields including medical and food industry. As both of these interactions can be simultaneously modified using ionic amphiphiles, the complexation of protein with amphiphiles has been employed to tune the sol-gel transitions. Anionic SDS prevents whereas nonionic C12E10 surfactant supports the protein gelation, The presence of SDS and C12E10 both, suppresses the SDS-induced resistance against the protein gelation. Small-angle neutron scattering study provides understanding of the mechanism responsible for these intriguing observations. It has been found that the suppression of hydrophobic attraction and enhancement of electrostatic repulsion inhibits the gelation of BSA-SDS complexes. Addition of C12E10 leads to the desorption of the SDS from protein and hence gives rise to protein gelation.

Physical Review Materials 7, 015601 (2023)

❖ Probing liquid-liquid phase separation and re-entrant behavior in nanoparticle-Pluronic system

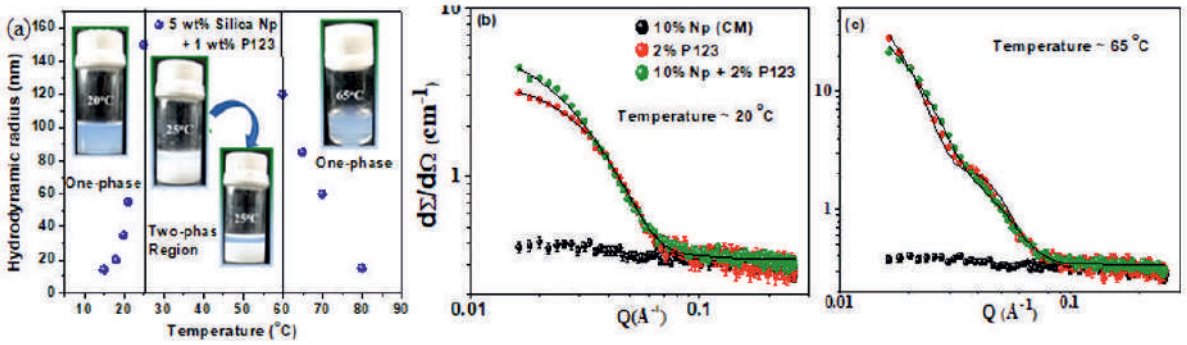

An interesting re-entrant liquid-liquid phase separation in silica nanoparticles-Pluronic (triblock copolymer, P123) suspension has been observed, where the system transforms from stable one-phase to two-phase (aggregate) and then return back to original phase on increasing temperature. The evolution of the interactions in nanoparticle-Pluronic system was examined by small-angle neutron scattering (SANS) and it has been shown that the Pluronic micelles adsorb on the nanoparticles and drives an attractive interaction among conjugates at lower temperatures, which finally leads to liquid-liquid phase separation at intermediate temperature. At high temperatures, Pluronic aggregates becomes highly hydrophobic, leading to detachment of Pluronic micelles from the nanoparticle surface and hence the re-entrant of the initial one-phase system.

Langmuir 39, 8109−8119 (2023)

❑ Selected Publications

1. S. Kumar, D. Saha, V. K. Aswal, Physical Review Materials 7, 015601 (2023).
2. R. Laishram, S. Sarkar, I. Seth, N.Khatun, V. K. Aswal, U. Maitra and S. J. George, J. Am. Chem. Soc. 144, 11306 (2022).
3. S. Kumar, D. Saha, D. Ray, S. Abbas, V. K. Aswal Phys. Rev. E (Letters) 104, L012603 (2021).
4. M. Sharma, V.K. Aswal, V. Kumar and R. Chidambaram, IUCrJ 7, 166-172 (2020).
5. A. Sikder, D. Ray, V. K. Aswal and S. Ghosh, Angew. Chem. Int. Ed. 58, 1606-1611 (2019).

Double crystal based SANS instrument

This is a double crystal based medium resolution small-angle neutron scattering instrument built and commissioned at the guide tube laboratory. The instrument consists of a non-dispersive (1, -1) setting of (111) reflections of silicon single crystals with sample between the two crystals.

Instrument parameters

Beam port	Guide G1
Monochromator	Si(111)
Wavelength	3.12 Å
$(\Delta\lambda/\lambda)$	~1 %
Flux at sample	500 n/ cm^2/sec
Analyser	Si(111)
Q range	0.0003 -0.0173 $Å^{-1}$
Real space resolution	200 - 10000 Å
Detector	BF_3
Sample environment	Multi-sample stage (Up to 5 samples) Heating stage (RT to 150°C)

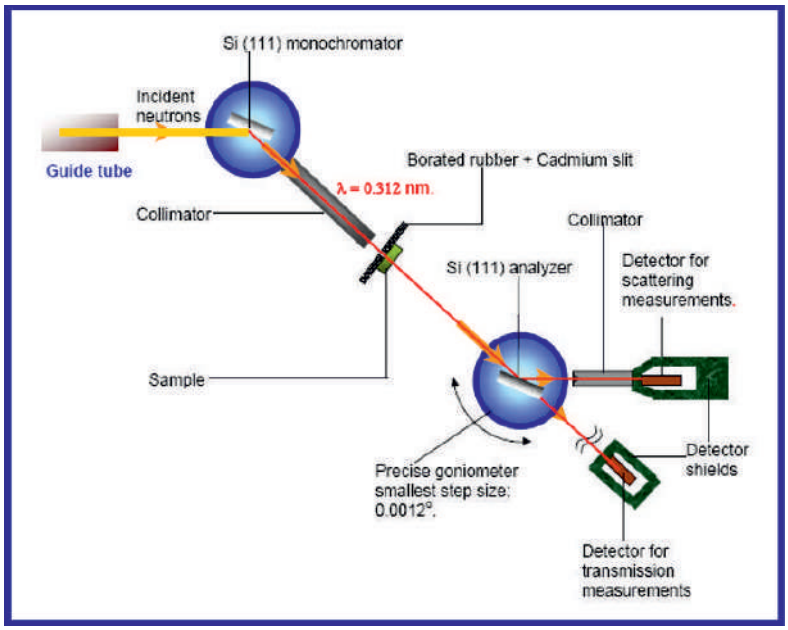

This facility is widely used to investigate the mesoscopic inhomogeneities in ceramics, metallurgical alloys, naturally occurring porous media like rock etc.

In this kind of double crystal based instruments, unlike pinhole collimation instruments, the collimation is performed in the reciprocal space only and the resolution in wave vector transfer Q is independent of the beam cross section. Because of the non-dispersive setting of both the crystals, the width of the rocking curve is independent of the divergence of the incoming beam.

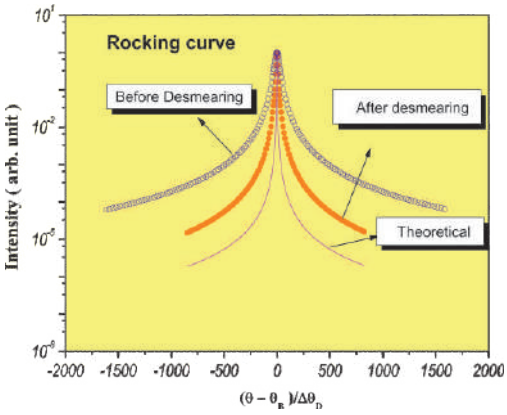

S. Mazumder, D. Sen, T. Saravanan and P. R. Vijayaraghavan, J. Neutron Research, **9**, 39 (2001).
S. Mazumder, D. Sen, T. Saravanan and P. R. Vijayaraghavan, Current Science, **81**,257-262 (2001) .

❑ Selected examples

❖ SANS unravels the hierarchical structure in dendritic fibrous silica nanospheres

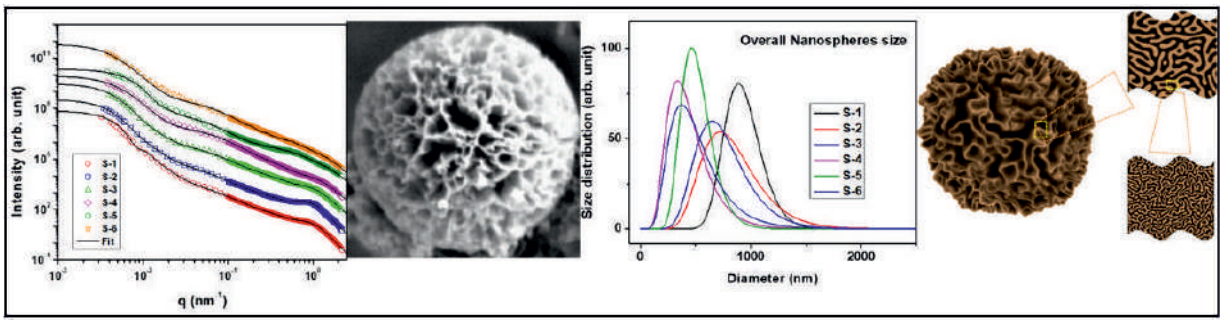

Templated nanomaterials play a crucial role in addressing technological challenges in several domains including energy, environment and health. In this regard, dendritic fibrous-nanosilica (DFNS) has shown immense potential for various applications primarily owing to its facile synthesis process, easily accessible surface area and up scalability but its complex structural hierarchy is still intriguing. The formation mechanism of such hierarchical pore morphology in these nanospheres is elucidated and it is observed that a relative variation in periodicity, sheet thickness, and their correlation significantly affects the specific surface area and pore structure, which is strongly influenced by hydrolysis rate and reaction time. Using MSANS data, a new length scale of the pores is discovered which was otherwise not visible by any other conventional technique. Evaporation induced assembly of such nano-silica with amine based polymers has shown tremendous potential for CO_2 capture.

Microporous and Mesoporous Materials, 323, 111234 (2021)

❖ SANS predicts the mechanism of shale formation

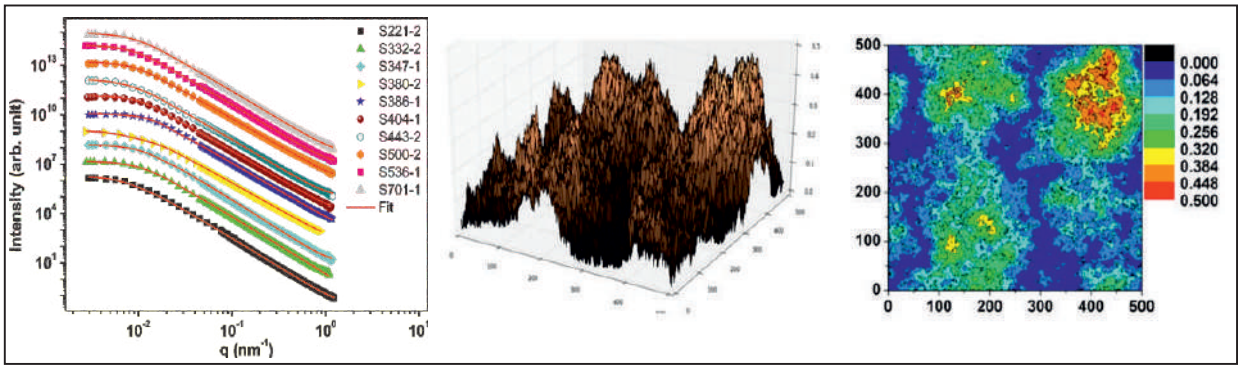

Shale gas exploitation in the United States has changed the energy dependency on imports and inspired exploration in Canada, China, Australia, and other countries. In an Indian context, potential for shale gas development exists in the Cambay basin in western India, the Krishna-Godavari basin along the east coast of India, the Cauvery basin in southern India, and the Damodar valley basin in eastern part of India. The Indian shales with varying mineral compositions and organic contents has been investigated in detail by ultra-small-angle neutron scattering and small-angle X-ray scattering. The variation of depth dependence fractal dimension of shales as revealed by SANS shows strong dependence on pore smoothening by the transport of the fluid over the long period of time which is corroborated by the Monte-Carlo based simulations. Further, the origin of high surface fractal dimension in shale observed by SANS is explained by the simultaneous deposition and dissolution under digenetic conditions. A vast amount of data related to pore morphology and porosity is generated using SANS which will be helpful to predict the shale gas storage capacity in Indian shale.

Int J Coal Geology 228, 103556 (2020)
Energy & Fuels 33 (6), 4835-4848 (2019)

❑ Selected Publications

1. D Sen, A Maity, J Bahadur, A Das, V Polshettiwar, Microporous and Mesoporous Materials, 323, 111234 (2021).
2. J Bahadur, S Mehta, S Singh, A Das, A Maity, T Youngs, D Sen, V Polshettiwar, Materials Advances 3 (16), 6506-6517 (2022).
3. V Vishal, D Chandra, J Bahadur, D Sen, B Hazra, B Mahanta, D Mani, Energy & Fuels 33 (6), 4835-4848 (2019).
4. D Chandra, V Vishal, J Bahadur, D Sen, International Journal of Coal Geology 228, 103556 (2020).
5. A Das, R Mondal, D Sen, J Bahadur, DK Satapathy, MG Basavaraj, Langmuir 38 (12), 3832-3843 (2022).

Polarized Neutron Reflectometer

Polarized neutron reflectivity (PNR) is a powerful non-destructive technique used to study morphology and magnetism of thin film heterostructures using both specular and off-specular reflectivity.

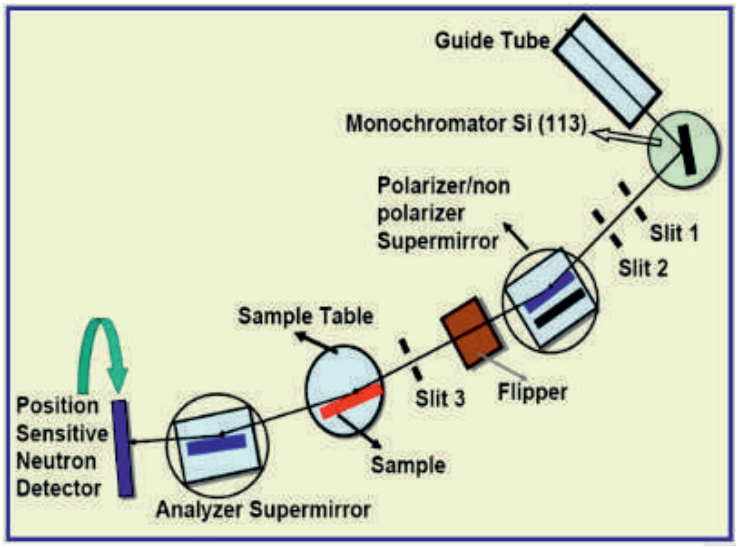

Instrument parameters

Beam port	Guide G1
Monochromator	Si (113)
Wavelength	2.9 Å
Polarizer	Fe/Si supermirror
Flux at Sample	10^4 n/ cm^2/sec
ΔQ/Q	0.141 – 0.411
Reflectivity	1 - 10^{-4}
DC Flipper Efficiency	93%
Detector	Linear ^{3}He PSD

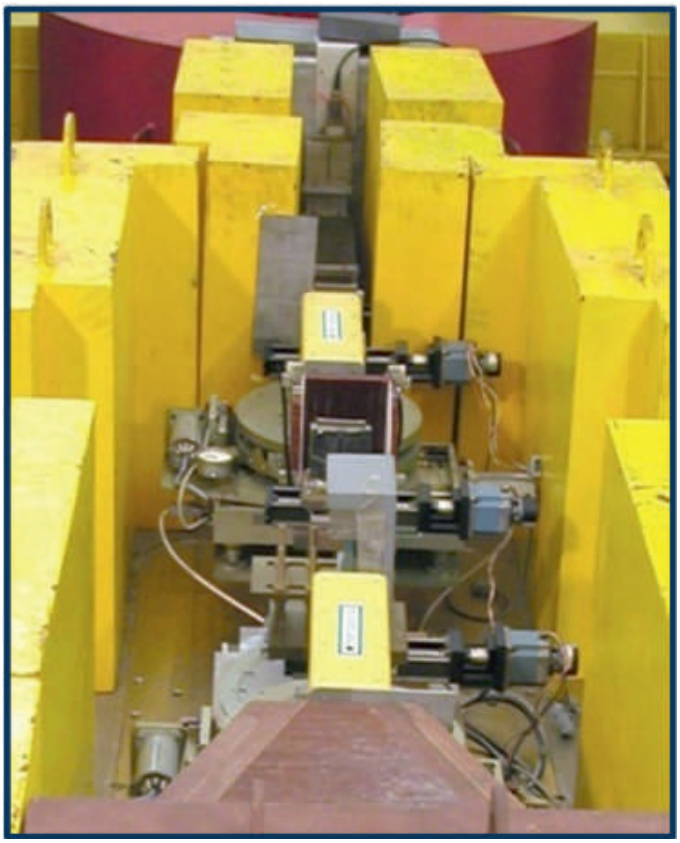

1. S. Basu and S. Singh, J. Neutron Res. 14, 109 (2006).
2. S. Singh, M. Swain, S. Basu, Prog. Mat. Sci. 96, 1 (2018).

The reflectometer has been designed for vertical sample geometry. It uses a linear position sensitive detector, which helps to collect both specular and off-specular reflectivity data from the thin film samples, in a single setting. Thermal neutrons have refractive index slightly less than unity, which makes their total external reflection possible at grazing angle of incidence making PNR an effective probe of surface and interface properties in thin films.

Reflectivity is intrinsically sensitive to the difference of the refractive index (or contrast) across any interface. For the case of specular reflection, the intensity of the reflected beam is related to the depth dependence of the index of refraction averaged over the lateral dimensions of the sample. This makes specular PNR a unique probe to study the depth-dependent structural, magnetic and interfacial properties of thin film heterostructures. Off-specular reflectivity is a widely used technique to understand surface (interface) morphology

❑ Selected examples

❖ Evidence of high density non magnetic cobalt phase at interfaces

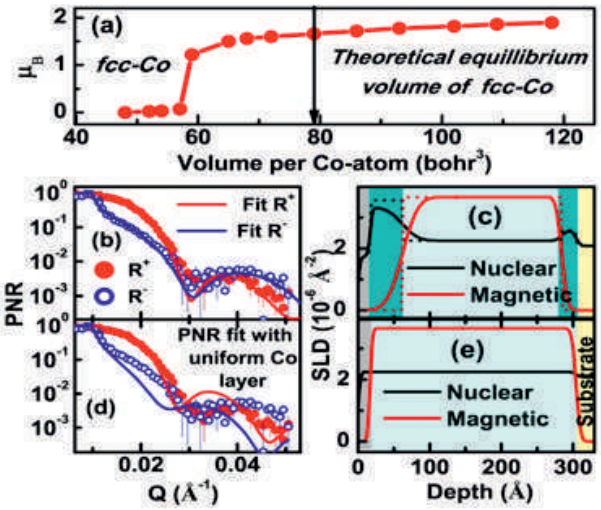

Existence of ultrathin superdense nonmagnetic cobalt layers in a polycrystalline cobalt thin film has been discovered. The densities of these layers are about 1.2–1.4 times the normal density of Co. This has been revealed by X-ray reflectometry experiments, and corroborated by PNR experiments.

The variation of magnetic moment as a function of volume, as suggested by theoretical prediction suggest zero moment for Co in *fcc* phase (top panel). PNR data from the film at room temperature were fitted considering different nuclear and magnetic depth profiles. Model with uniform Co density with uniform magnetization does not fit the PNR data (bottom panel). PNR results predicted high density Co layer at both interfaces, which has nearly zero magnetic moment density (middle panel).

Scientific Reports, 7, 41856 (2017)

❖ Interface morphology driven exchange interaction and magnetization reversal in a Gd/Co multilayer

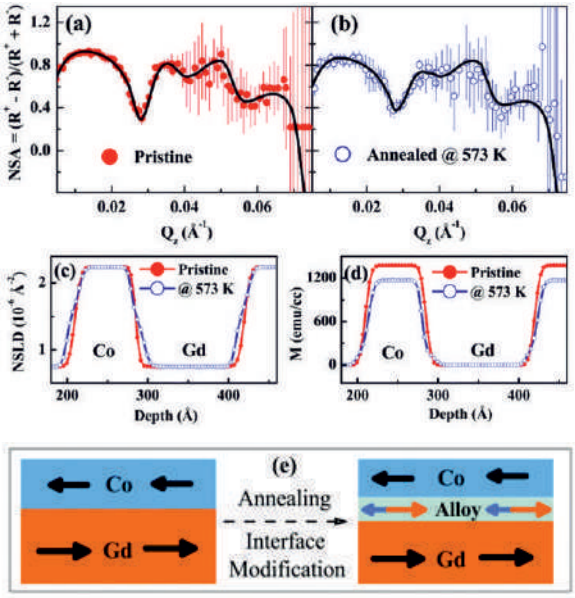

Interface morphology driven structural and magnetic properties of a Gd/Co multilayer were investigated. The interface morphology was varied by annealing the multilayer sample. PNR in conjunction with other relevant experimental techniques and a simple one-dimensional spin-based model calculation, suggested a strong interface dependent exchange coupling.

PNR data (upper panel), represented in terms of normalized spin asymmetry (NSA), and its best fit for pristine and annealed multilayers. The nuclear and magnetic scattering length density (NSLD and MSLD) depth profiles obtained from the PNR data (middle panel) indicate modulation near the interface on annealing. In addition, the MSLD depth profile shows reduced magnetization in the Co layer on annealing the multilayer sample. This is attributed to emergence of a non-magnetic alloy layer at the interface. Representation of the exchange interaction at interfaces of Co/Gd bilayer before and after annealing (lower panel).

Phys. Chem. Chem. Phys., 24, 6580 (2022)

❑ Selected Publications

1. P. Negi, M. Gupta, R. Rawat, R. Joshi, H. Bhatt, S. Singh, V.R. Reddy, H. Kumar, J. Magn. Magn. Mater. 581, 170941 (2023).
2. D. Bhattacharya, V. Karki, S. Singh, T.V.C. Rao, Appl. Surf. Sci. 572, 151300 (2022).
3. S. Singh, M.A. Basha, H. Bhatt, Y. Kumar, M. Gupta, Phys. Chem. Chem. Phys. 24, 6580 (2022).
4. S. Singh, H. Bhatt, Y. Kumar, C.L. Prajapat, A. Mishra, S. Bedanta, S. Basu, Appl. Surf. Sci. 570, 151193 (2021).
5. M.A. Basha, H. Bhatt, Y. Kumar, C. L. Prajapat, M. Gupta, S. Basu, and S. Singh, Materials Letters 283, 128879 (2021).

Triple Axis Spectrometer

Triple axis spectrometer is used to study Inelastic Neutron Scattering from single crystals and polycrystalline samples.

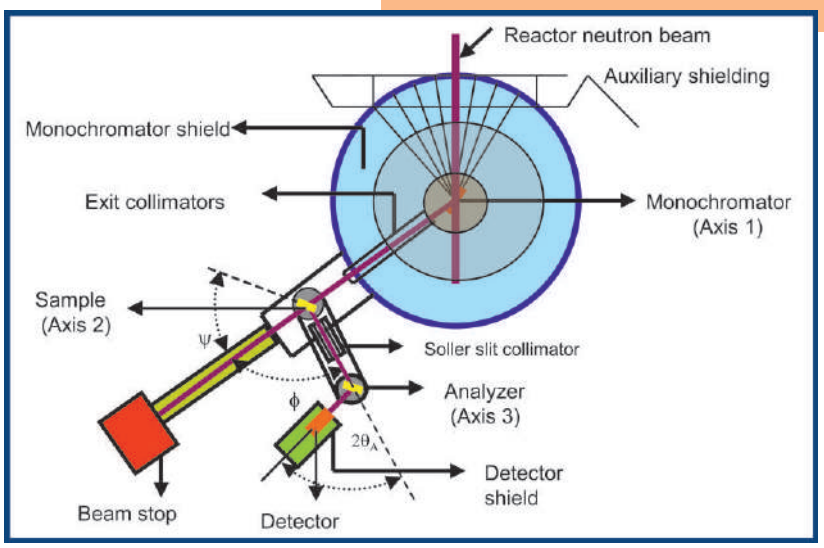

Instrument parameters

Beam port	T1007
Monochromator	Doubly Focussing Cu(111)
Energy Transfer range	3 - 150 meV
Momentum transfer range	1 – 7 $Å^{-1}$
Incident neutron Wavelength range	0.6 – 2.3 Å
Beam size	40 mm x 40 mm
Flux at sample (maximum)	10^6 n/cm^2/s
Analyzer	PG (0002)
Filter	PG
Scattering angle	10^o – 100^o
Detector	^{3}He counter
Sample environment	CCR (4 K – 300 K)

This instrument has been successfully employed for measurements of phonon dispersion curves, phonon density of states, crystal field excitations and quasielastic scattering.

Principal components of this instrument are:
(i) Monochromator that produces the mono-energetic neutron beam.
(ii) Positional spectrometer that sets the angles.
(iii) Analyzer that measures the outgoing energy.
Various arms of the spectrometer can be moved at angular speeds of several degrees/ minute by means of worm-gear assemblies.

The geometry of the triple axis spectrometer allows measurement of the scattering function S(Q, E) in single crystals at well defined values of momentum transfer Q and energy transfer E.

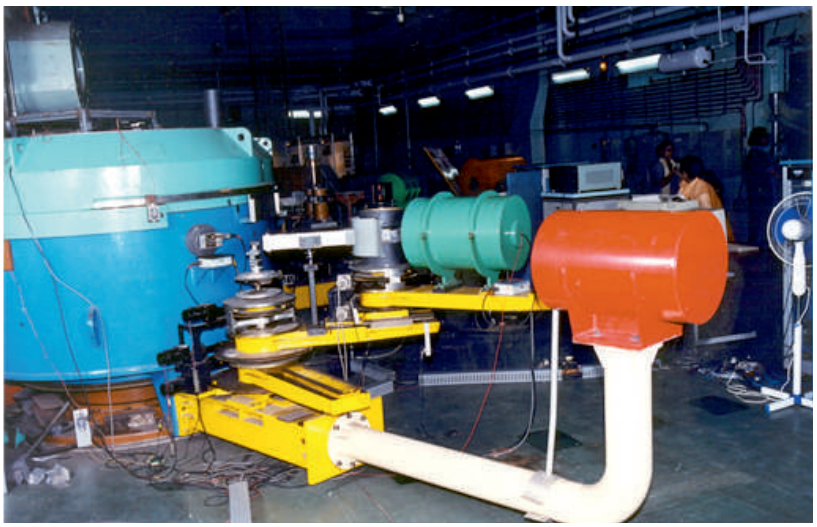

S.L. Chaplot, R. Mukhopadhyay, P.R. Vijayaraghavan, A.S. Deshpande, and K.R. Rao, Pramana – J. Phys. 33, 595 (1989).

❑ Selected examples

❖ Dynamics of atoms in thermoelectric Cu_2ZnSnS_4

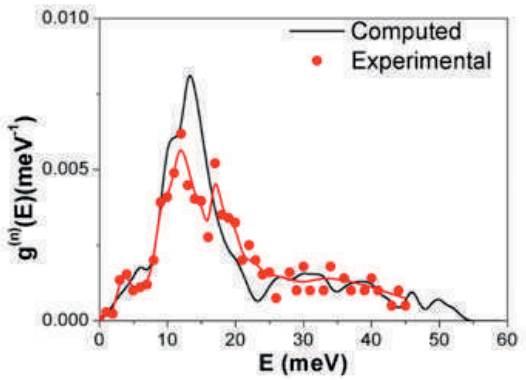

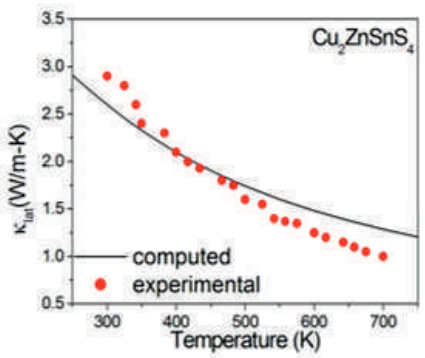

Most thermoelectric materials now available are tellurides or antimonides of transition metals or contain rare earth elements. Cu_2ZnSnS_4 is a thermoelectric material with earth abundant elements, and a non-toxic composition.

Computational validation of the experimental phonon density of states helped to estimate the lattice contribution to thermal conductivity.

J Phys Chem Solids 150 ,109819 (2021)

❖ Phonons and Anisotropic Thermal Expansion Behaviour of NiSe, and NiSi

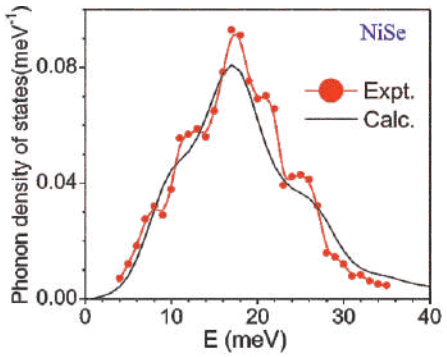

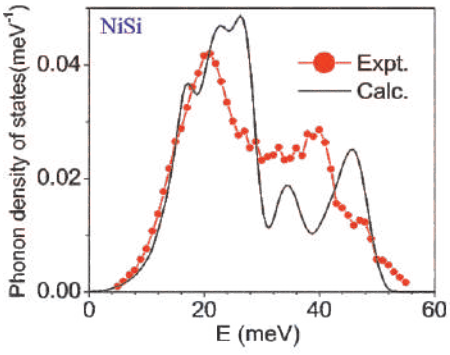

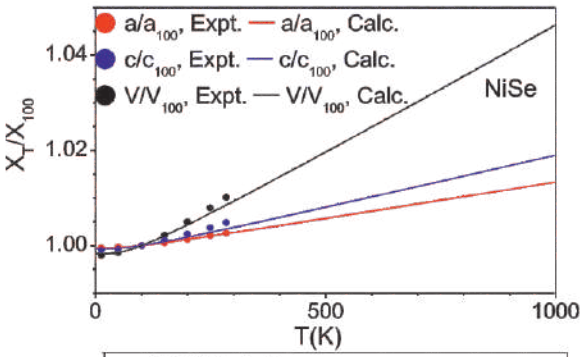

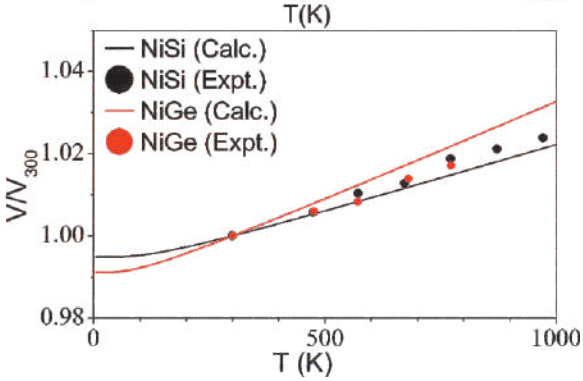

Computational validation of the experimental phonon density of states helped to understand anisotropic thermal expansion behaviour in NiSi and NiSe.

Frontiers in Chemistry 6, 2296 (2018)
Journal of Applied Physics 125, 205106 (2019)

❑ Selected Publications

1. P. Goel et al, Frontiers in Chemistry 6, 2296 (2018).
2. P. Goel et al, Journal of Applied Physics 125, 205106 (2019).
3. S. P. Kandare et al., J Phys Chem Solids 150 ,109819 (2021).

Quasi elastic Neutron Spectrometer

This is a double crystal based multi-angle reflecting x-tal (MARX) quasielastic neutron scattering (QENS) instrument built and commissioned at the Dhruva reactor hall. It uses a single crystal analyzer for measuring energy transfer.

Instrument parameters

Beam port	TT1004
Monochromator	PG(0002)
Two monochromators (size: 100 × 80 mm^2) are used in tandem (2nd one vertically focussed for higher flux on sample)	
Wavelength	1.3 – 4.7 Å
(ΔE/E)	~4 % (200 μeV with incident wavelength 4 Å)
Flux at sample	5 x 10^5 n/cm^2/sec
Analyser	PG(0002)
Q range	0.6 – 1.8 Å^{-1}
Scattering angle	2θ < 80º
Detector	^{3}He gas detector

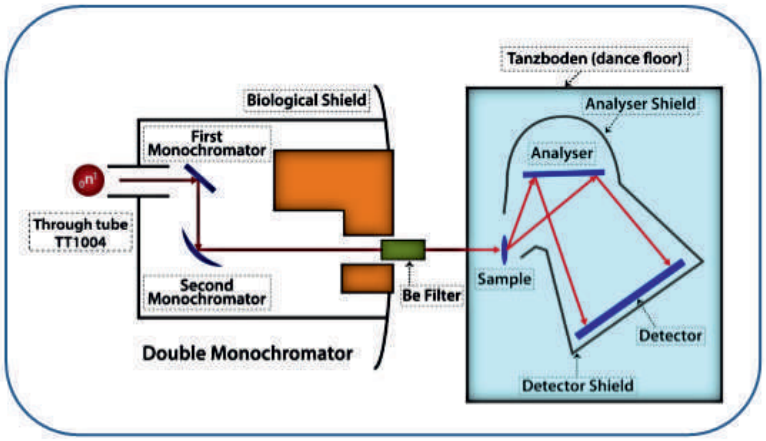

- By virtue of double monochromator, neutrons of different incident energy can be obtained at a fixed sample position.
- The instrument works in Multi angle Reflecting X-tal (MARX) mode thereby facilitating complete energy spectrum for one instrumental configuration.
- Provision to change the distance between different axes to obtain different energy resolutions.
- The out-of-pile portion of the instrument is on a 'tanzboden' facilitating easy maneuvering.

Quasi elastic spectrum

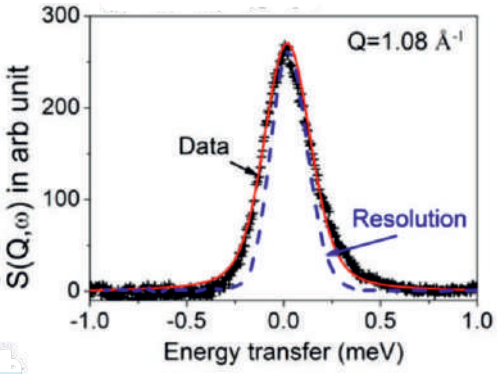

R. Mukhopadhyay, S. Mitra, S. K. Paranjpe, B. A. Dasannacharya, Nuclear Instruments and Methods in Physics Research A 474, 55-66 (2001).

❑ Selected examples

❖ Role of cholesterol in microscopic dynamics of metallosome-based membranes

QENS spectra

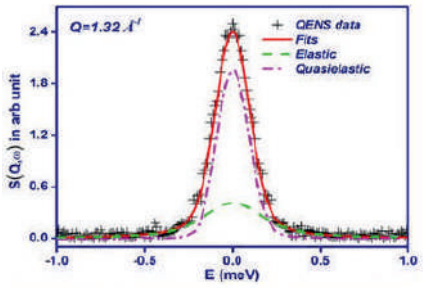

The model for localised diffusion of atoms along the chain of the metallosurfactants – varying dynamical size with chain length

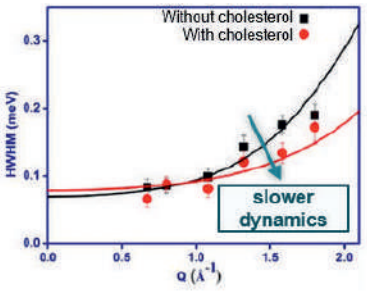

J. Mol. Liq. 318, 114034 (2020)

The controlled stoichiometry of single-tailed surfactant cetylpyridiniumchloride (CPC) in the presence of Cu ions led to a vesicular assembly known as 'metallosomes'. The fluidity of these systems are controlled by addition of cholesterol to make them suitable for targeted drug-delivery.

Addition of cholesterol stiffens the membrane – QENS analysis reveals that cholesterol arrests the dynamics of metallosurfactants in the vesicle.

❖ Water enhances the diffusion of acetamide molecules in deep eutectic solvents

QENS spectra

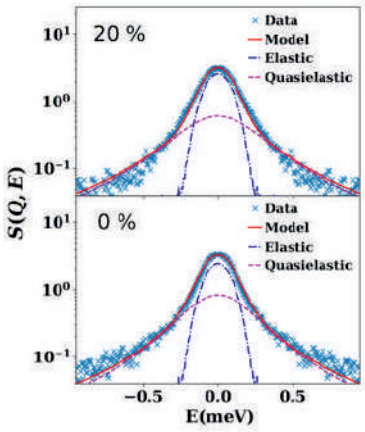

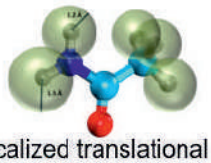

Localized translational diffusion (LTD)

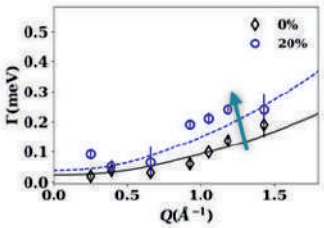

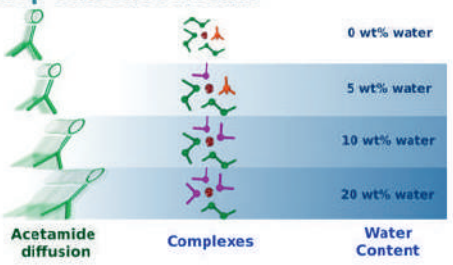

The diffusion of acetamide – both localized and jump diffusion is enhanced by addition of water

J. Phys. Chem. B 126, 9026 (2022)

Enhanced acetamide diffusion is due to the change in solvation structure of Li+ ions – important for Li-ion batteries.

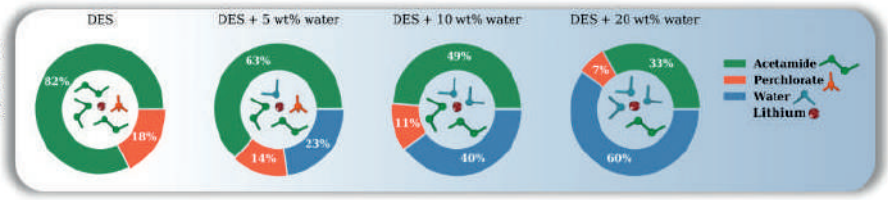

❑ Selected Publications

1. H. Srinivasan, V. K. Sharma, S. Mitra, R. Biswas and R. Mukhopadhyay, Physica B 562 13 (2019).
2. H. Srinivasan, V. K. Sharma, R. Mukhopadhyay and S. Mitra, J. Chem. Phys. 153 104505 (2020).
3. B. Kaur, G. Kaur, G. R. Chaudhary, V. K. Sharma, H. Srinivasan, S. Mitra, A. Sharma, S. L. Gawali, and P. A. Hassan, J . Mol. Liq. 318 114034 (2020).
4. H. Srinivasan, V. K. Sharma and S. Mitra, Phys. Chem. Chem. Phys. 23 22854 (2021).
5. H. Srinivasan, V. K. Sharma and S. Mitra, J. Phys. Chem. B 126 9026 (2022).

Time of Flight Spectrometer

This instrument is used to study Inelastic Neutron Scattering from condensed matter

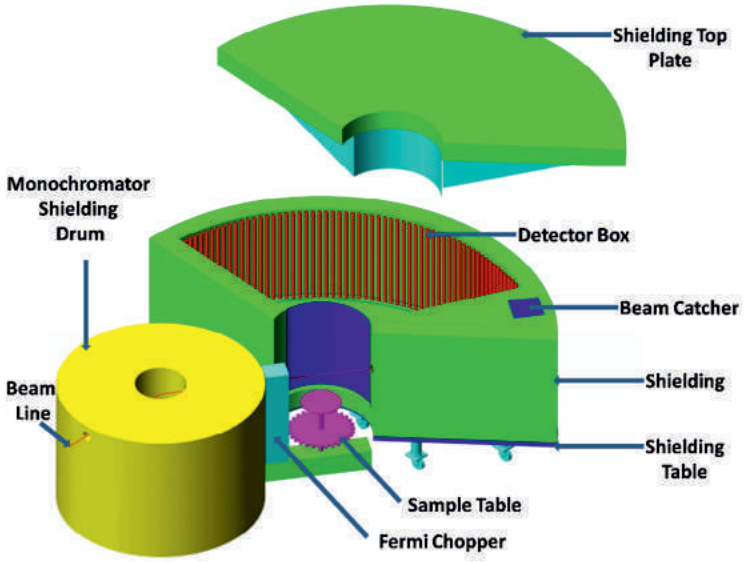

Instrument parameters

Beam port	HS1017
Monochromator	Doubly Focussing Cu(111)
Energy Transfer range	3 - 150 meV
Momentum transfer range	1 – 7 $Å^{-1}$
Incident neutron Wavelength	1.2 Å
Beam size	40 mm x 40 mm
Flux at sample (maximum)	10^6 n/cm^2/s
Analyzer	Time of Flight
Scattering angle	40^o – 100^o
Detectors	^{3}He position sensitive
Sample environment	CCR (4 K – 300 K)

Neutrons from the reactor strike a crystal monochromator.
The monochromatic beam is then pulsed by a chopper placed at a known distance from the sample.
An array of detectors is arranged at a known fixed distance from the sample, and scattered neutrons arrive at the detectors at times determined by their scattered energies.

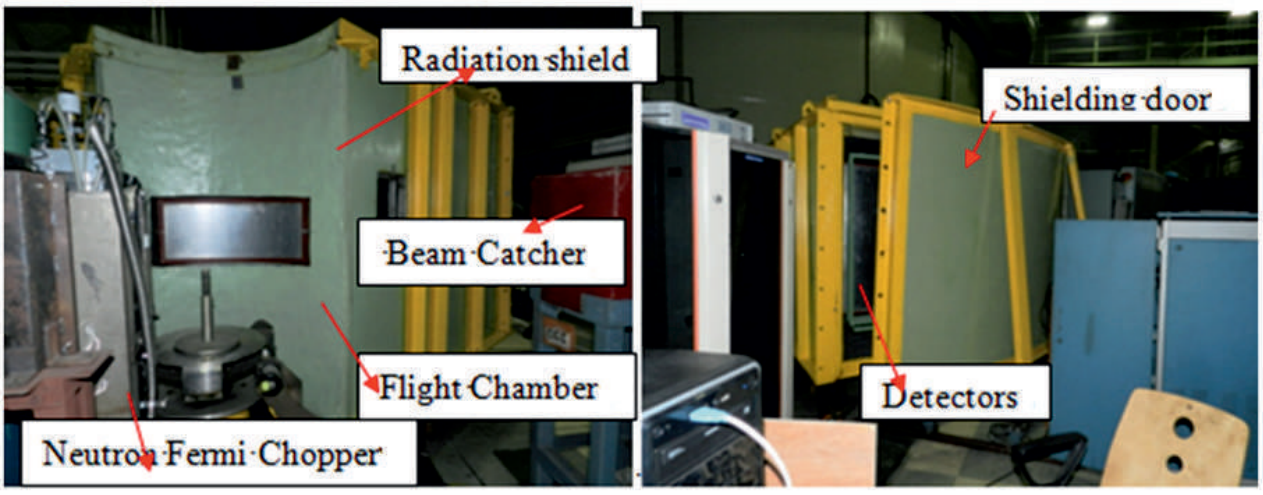

Mala N. Rao, Shraddha S. Desai, Rohit Chandak, S. S. Naik, V. Kulkarni, S. K. Mishra, Santosh Kumar, S. Mitra, P. Goel, R. Mittal, Somesh Rai, R. Mukhopadhyay, and S. L. Chaplot, Proc. Solid State Phys. Symposium 55, 358 (2021).

❑ In-house developments

❖ Position Sensitive Detectors

The position sensitive detectors (PSDs), developed in-house are arranged vertically and allow large solid angle coverage. The PSDs are with coaxial geometry and completely welded cathode in SS and 25 µm diameter of resistive anode (NiCr). 20 PSDs are filled with gas ^{3}He (2 bar) + Kr (1.5 bar) and 20 PSDs are with 1.1 bar BF_3 gas. Two PSDs are looped to treat it effectively as a single PSD. This arrangement reduces the number of electronic modules needed to half. These PSDs (Position resolution 6 mm FWHM) have uniform operating parameters; which suits the looping arrangement.

❖ Timer Circuit

The Fermi chopper controller has a BNC output on the front panel which gives a once per revolution signal. This chopper pulse starts the reference timer and the periodic time window ticks generated by the timer circuit defines the time window (here 1µs) and are used for measurement of flight time of neutrons detected in all the PSDs.

❖ Data Acquisition Module

The charge division method is employed for position encoding. The time of arrival of neutron with respect to the zero-time pulse is used to estimate its energy and build histogram of scattered neutrons. A five channel NIM module caters to these needs.

❑ Phonons in vanadium, and ammonium chloride

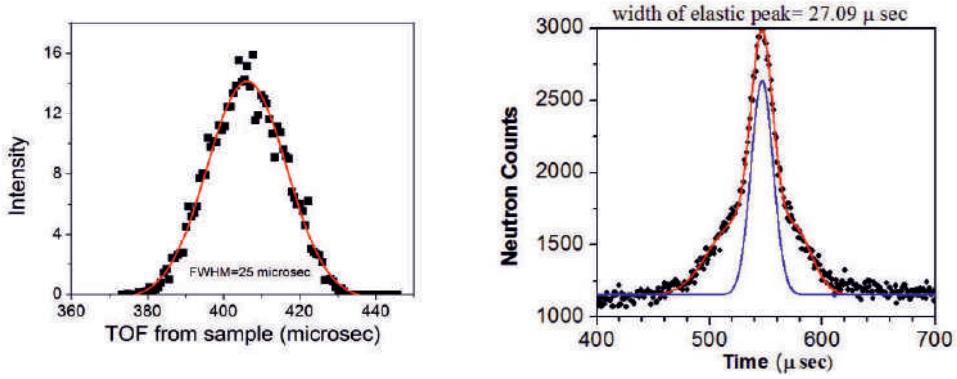

Elastic resolution of 27 µsec matches with the computed value, giving an energy resolution ~ 5 meV

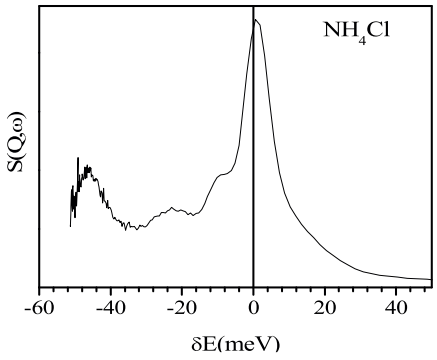

The elastic peak is followed by a continuous spectrum and two peaks at energy transfers of 24 meV and 48 meV correspond to the translational and librational modes of the NH_4 ion respectively

NFNBR

Neutron Detectors Development Facility

NFNBR at Dhruva reactor is equipped with indigenously developed neutron detectors. SSPD has shown considerable growth in development of ^{3}He and BF_3 filled neutron detectors over the years. Various types of neutron detectors developed range from neutron beam monitors, proportional counters, 1-Dimensional and 2-D Position Sensitive Neutron detectors (PSD). All the detectors developed in-house have shown stable operation and long life over years.

Detector development facility also caters to other DAE units with tailor-made, user specific designed detectors for special applications. Such detectors are not available commercially in the global market. High efficiency and high-resolution PSDs have resulted in state of art scientific research making optimal use of neutron beam.

Applications: Neutron scattering, flux monitoring, area monitoring, nuclear waste monitoring, and characterization of pulsed neutron sources.

Various types of neutron and X-ray detectors developed by Solid State Physics Division

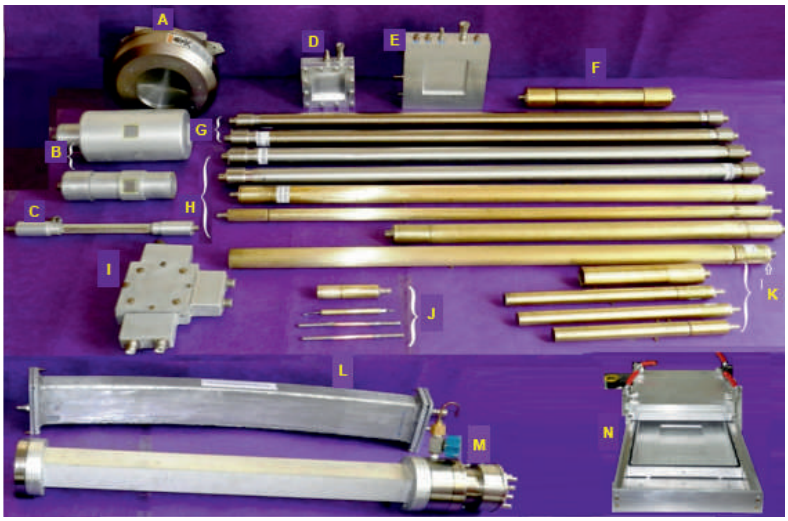

A) Multiwire 2D PSD for X-Rays
B) X ray Proportional counter
C) 1D PSD for X Ray
D) Neutron Beam Monitor (Counting)
E) Neutron Beam Imaging Monitor (2D PSD)
F) 1D PSD neutron for Reflectometer
G) 1D PSD (BF_3 filled) for neutron TOF
H) 1D PSD (^{3}He filled)
I) Microstrip based neutron PSD
J) Neutron flux monitor counters
K) Neutron Proportional counters
L) ^{10}B coating based Multigrid neutron PSD
M) Multitube Neutron PSD (BF_3 filled)
N) 2π counting chamber for Large area α-β sources.

Large area Two-Dimensional position sensitive detector (2D PSD)

A large area 2D neutron PSD (650 mm x 650 mm) has been designed. It consists of a ^{3}He gas filled chamber enclosing three orthogonal multiwire grids: Anode, X and Y cathode.

Automated Grid Winding Machine with multiwire PCB mounting frame, Linear Motion guide with control panel

2D PSD for neutrons with 650 mm x 650 mm sensitive area, PSD enclosure with vacuum system

Tailor-made detectors for specific applications

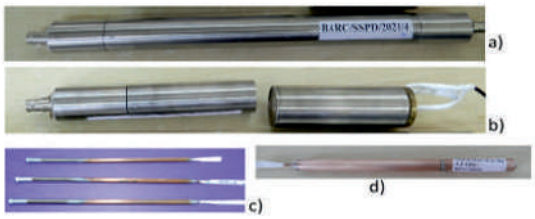

a) BF_3 filled detector for FRENA at SINP, Kolkata and RMP, Mysuru b) Neutron area monitors for Dhruva reactor c) Miniature neutron detectors for BRAHMMA neutron generator, d) Neutron detector for portable D-D neutron source e) Neutron beam monitors in planar and coaxial geometry

2D imaging beam monitor with delay line-based position readout and sensitive area 10 cm x 10 cm

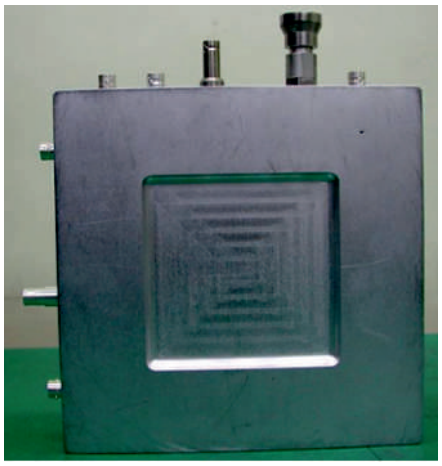

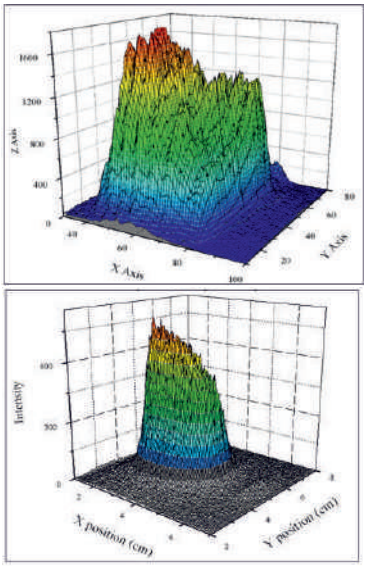

Neutron beam intensity mapping of beams at Dhruva reactor

Multi PSDs mounted in Fan-like arrangement for near-2D detection

Multipurpose test facility at Guide G2

Automated X-translation at Guide G2 for precision shift of PSD

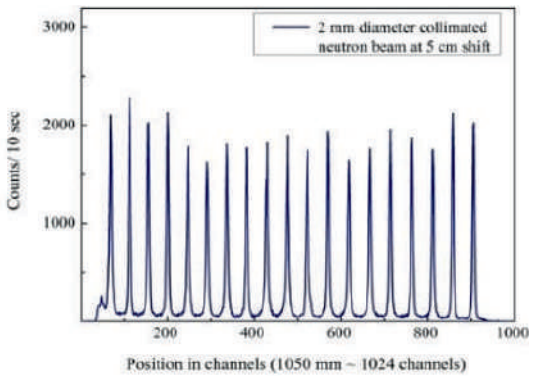

Position scan of a PSD (50 mm beam shift)

Effect of temperature on performance of Boron Trifluoride (BF_3) gas-based neutron proportional counters, Shraddha S. Desai, Mala N. Rao, Radiation Measurements 144, 106593 (2021).

Control and Instrumentation Laboratory

The instrumentation and control of neutron scattering experiments involve the following aspects: (A) Experiment Control and Data Acquisition Software, (B) Motor Position Control Systems,

(C) Nuclear Electronics for Neutron Counting, (D) Sample Environment Equipment. Various systems and modules used in these set ups are either commercial off-the shelf items or developed in-house.

Experiment Control and Data Acquisition Software

This software receives user's inputs to initialize the experiment run, do motor control operations with the help of hardware motor position control units, integration with sample environment systems to record data under various sample temperature or magnetic field, record display and save data.

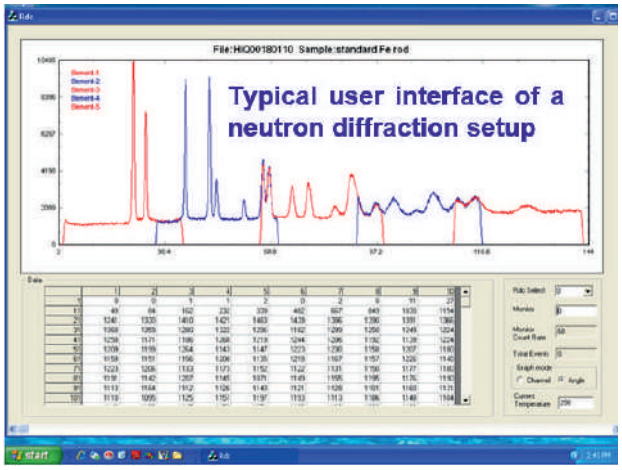

Internal view of a motor position control electronics

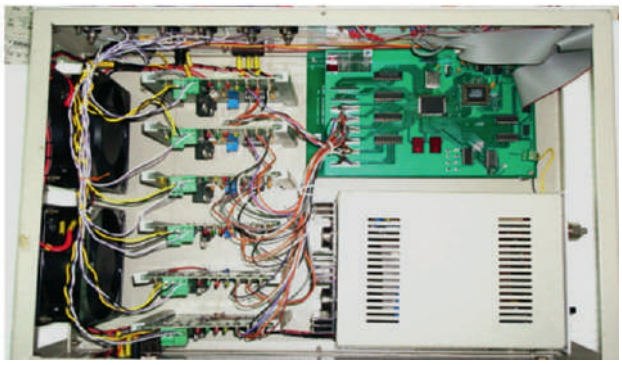

Motor Position Control Systems

These systems are pervasively used in neutron scattering experiments for alignment of various arms/axis of neutron spectrometers, sample changers, collimators, focusing devices etc. The functional objective of motor control is collectively achieved by the motor control and communication classes in the software stack and the microcontroller and/or FPGA based control hardware. There controller cards drive the H-bridge circuit and take inputs from feedback devices such as encoders, servo pots and limit switches.

Nuclear Electronics for Neutron Counting

The neutron detectors are used in two modes (a) end-on mode and (b) position encoding mode. In the end-on mode where the interest is only in counting events, while the position encoding mode uses neutron Position Sensitive Detector (PSD). The front-end nuclear electronics needed for these modes are: (1) Charge sensitive pre-amplifiers (PA), (2) Shaping amplifiers (SA), (3) Scalar counter timer module, (4) Position encoding electronics also called Ratio to Digital Converters (RDC), (5) Data acquisition modules called PSD Data Recording module.

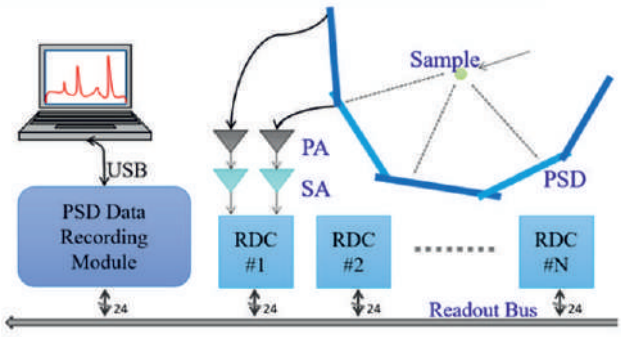

Y.S. Rana, Tej Singh, V. Kulkarni, R.M. Chandak, S.S. Desai, S.S. Naik and Mala N. Rao, Report BARC 2019/E/007 (2019).

Control and Instrumentation Laboratory

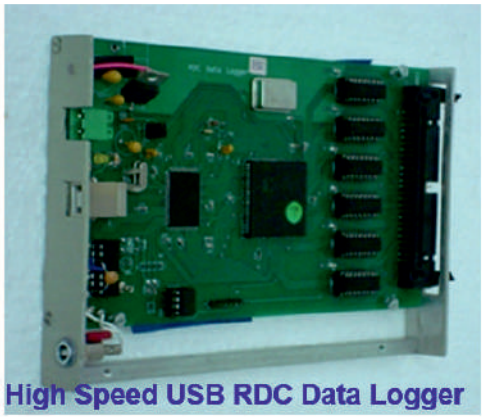

High Speed USB RDC Data Logger

Ratio to Digital Converter (RDC)

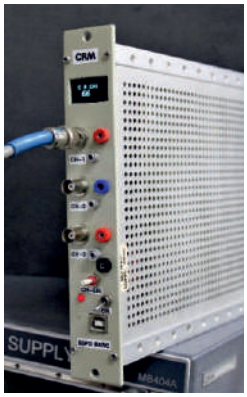

3-Channel Count Rate Module

It is a single width NIM module which gives the count rate so that the instrument user is able to track the peak intensity position of the detectors with ease as the motor scans between any two positions. It shows the real-time count rate (counts per second) in different positions of the motor. It can display the count rate of three different channels and the channel selection is done by the selector switch on the front panel of the module.

Scaler Discriminator Module

A Scaler Timer Module is a data acquisition unit which can be used in step-scan type-based instruments, i.e., neutron scattering instruments where end-on detectors are used. It takes the Quasi Gaussian pulse as input and gives us the total counts (digital) of each of the channels. The total time for which the counts are to be taken is selected via the front panel. A scaler switch at the back panel allows scaling down of the counts by 1,10,100,1K and 10K. It has the following provisions for connecting to the computer: RS232 & USB.

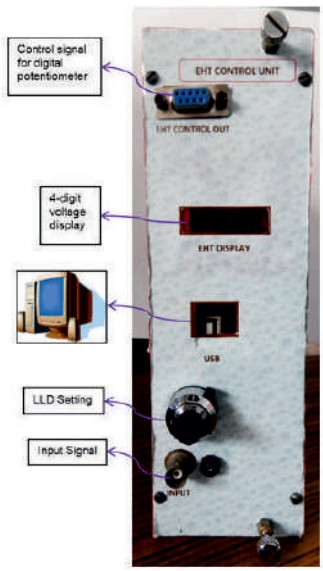

Automated Anode Bias Curve Recording Module For Proportional Neutron Detectors

This module plots the counts as a function of voltage and helps to find the operating voltage of neutron proportional counters. Since it is a single portable module, it can be taken to any experimental set up for on-site characterization of proportional neutron detector and minimal manual intervention is required during the characterization process.

Stand-alone data acquisition (DAQ) module for step-scan based instruments in Dhruva under National Facility for Neutron Beam Research (NFNBR), Sanjeev Kumar Poudel, Santosh Kumar, S.S. Naik, Rohit M. Chandak, V.B. Kulkarni, S.S. Desai and Mala N. Rao, Report BARC/2023/E/010 (2023).

NFNBR

Contact Scientists

Location	Facility	Persons responsible	Office Address	Contact Ext. No.	Email address
T1007	Triple Axis Spectrometer (TAS)	1. R Mittal 2. P Goel 3. M K Gupta	R No 45, CIRUS R No 87, Dhruva R No 87, Dhruva	24307 26235 29128	rmittal@barc.gov.in knp@barc.gov.in mayankg@barc.gov.in
T1009	Polarized Neutron Spectrometer (PNS)	1. Amit Kumar 2. Anil Jain 3. K Chikara	R No 87, Dhruva R No 89, Dhruva R No 78, Dhruva	26273 27023 26200	amitkr@barc.gov.in ajain@barc.gov.in kchikara@barc.gov.in
T1011	Single Crystal Diffractometer (SCD)	1. R Chitra 2. Rajul Choudhury	R No 307, CMPD Building	24623	rchitra@barc.gov.in rajul@barc.gov.in
TT1015	Powder Diffractometer-1 (PD - 1)	1. A K Bera 2. Amit Kumar 3. Anil Jain	R No 78, Dhruva R No 87, Dhruva R No 89, Dhruva	26200 26273 27023	akbera@barc.gov.in amitkr@barc.gov.in ajain@barc.gov.in
T1013	Powder Diffractometer-2 (PD - 2)	1. S K Mishra 2. S Wajhal 3. A B Shinde	R No 87, Dhruva	26287 24306 24306	skmsspd@barc.gov.in swajhal@barc.gov.in abshinde@barc.gov.in
TT1015	Powder Diffractometer-3 (PD - 3)	1. S D Kaushik 2. S Rayaprol 3. P D Babu	R No 61, R5 Shed R No 246-C, CFB R No 246-C, CFB	24931 27112 24930	sdkaushik@csr.res.in sudhindra@csr.res.in pdbabu@csr.res.in
HS1017	Time of Flight Spectrometer (TOF)	1. Mala N Rao	R No 8, Dhruva	25606	mala@barc.gov.in
HS1019	High-Q Diffractometer (Hi - Q)	1. S Wajhal 2. S K Mishra 3. P S R Krishna	R No 89, Dhruva R No 89, Dhruva R No 8, Dhruva	24306 26287 25612	swajhal@barc.gov.in skmsspd@barc.gov.in glass@barc.gov.in
TT1004	Quasi Elastic Neutron Spectrometer (QENS)	1. S Mitra 2. V K Sharma 3. Harish Srinivasan	R No 12, Dhruva R No 87, Dhruva R No 78, Dhruva	24674 24604 24292	smitra@barc.gov.in sharmavk@barc.gov.in harishs@barc.gov.in
G1-1	Small-Angle Neutron Scattering Diffractometer (SANS - 1)	1. Sugam Kumar 2. Debes Ray 3. Sohrab Abbas	R No 44, CIRUS R No 45, CIRUS R No 44, CIRUS	24606 26282 24606	sugam@barc.gov.in debes@barc.gov.in abbas@barc.gov.in
G1-2	Polarized Neutron Reflectometer (PNR)	1. Surendra Singh 2. D Bhattacharya 3. Harsh Bhatt	R No 12, Dhruva R No 309, CMPD R No 78, Dhruva	24659 24070 24292	surendra@barc.gov.in debarati@barc.gov.in harshbhatt@barc.gov.in
G1-3	Double crystal-based SANS instrument (SANS - 2)	1. Debasis Sen 2. J Bahadur 3. Avik Das	R No 44, CIRUS R No 44, CIRUS R No 44, CIRUS	24608 26281 29146	debasis@barc.gov.in jbahadur@barc.gov.in avikd@barc.gov.in
G2	Multipurpose Test Facility	1. S S Desai 2. Mala N Rao	R No F-10, Hall 4 R No 8, Dhruva	22021 25606	ssdesai@barc.gov.in mala@barc.gov.in

List of conversion factors used in neutron scattering

(The table is to be read horizontally, e.g. λ = 1 Å corresponds to v = 3956 m/s or to E = 81.807 meV, etc.)

	kJ/mol	kcal/mol	meV	cm^{-1}	rad/sec	Hz	K	Å	m/sec
kJ/mol	1	0.2388	10.36	83.58	1.574×10^{13}	2.505×10^{12}	120.3	2.810	1.408×10^{3}
kcal/mol	4.187	1	43.39	345.0	6.591×10^{13}	1.049×10^{13}	503.3	1.373	2.881×10^{3}
meV	0.097	0.0230	1	8.006	1.519×10^{12}	2.418×10^{11}	11.605	9.045	437.4
cm^{-1}	1.196×10^{-2}	2.858×10^{-3}	0.124	1	1.884×10^{11}	2.98×10^{10}	1.439	25.68	154.05
rad/sec	6.351×10^{-14}	1.517×10^{-14}	6.582×10^{-13}	5.309×10^{-12}	1	0.159	7.640×10^{-12}	1.115×10^{7}	3.547×10^{-4}
Hz	3.991×10^{-13}	9.536×10^{-14}	4.136×10^{-12}	3.336×10^{-11}	6.238	1	4.800×10^{-11}	4.447×10^{6}	8.895×10^{-4}
K	8.314×10^{-3}	1.986×10^{-3}	8.616×10^{-2}	0.695	1.309×10^{11}	2.083×10^{10}	1	30.81	128.4
Å	7.894	1.885	81.807	659.8	1.243×10^{14}	1.978×10^{13}	949.4	1	3.956×10^{3}
m/sec	5.044×10^{-7}	1.202×10^{-7}	5.227×10^{-6}	4.216×10^{-5}	7.948×10^{6}	1.265×10^{6}	6.066×10^{-5}	3.956×10^{3}	1

Quantity	Symbol	Unit	
Energy	E	kJ, kcal, meV	
Optical wave vector	ν/c	cm^{-1}	
Cycles	ω	rad/sec	$E=\hbar\omega$
Frequency	ν	Hz	$\nu=\omega/2\pi$
Temperature	T	K	$E=k_BT$
Wavelength	λ	Å	$E=h^2/(2m\lambda^2)$
Velocity	v	m/sec	$E=mv^2/2$

m=1.674954·10 $^{-27}$ kg; $\lambda \propto 1/\sqrt{E}$; $v \propto \sqrt{E}$; $k \propto \sqrt{E}$

Typical values for cold, thermal and epithermal neutrons

	Energy	Wavelength	Wave vector	Velocity	Frequency
Cold neutrons	E = 1 meV	λ= 9.0446 Å	k = 0.6947 1/Å	v = 437 m/s	ν = 0.2418 THz
	E = 5 meV	λ= 4.0449 Å	k = 1.5534 1/Å	v = 978 m/s	ν = 1.2090 THz
Thermal neutrons	E = 25 meV	λ= 1.8089 Å	k = 3.4734 1/Å	v = 2187 m/s	ν = 6.045 THz
	E = 50 meV	λ= 1.2791 Å	k = 4.9122 1/Å	v = 3093 m/s	ν = 12.090 THz
Epithermal neutrons	E = 500 meV	λ= 0.4045 Å	k = 15.533 1/Å	v = 9780 m/s	ν = 120.89 THz
	E = 1000 meV	λ= 0.2860 Å	k = 21.968 1/Å	v = 13831 m/s	ν = 241.79 THz

NFNBR

For further information about facilities and proposals for experiments, contact:

Head, Solid State Physics Division
Bhabha Atomic Research Centre
Mumbai - 400085, India
Telephone : +91 22 25593757 / 5376
Fax : +91 22 25505151
Email : sspd@barc.gov.in

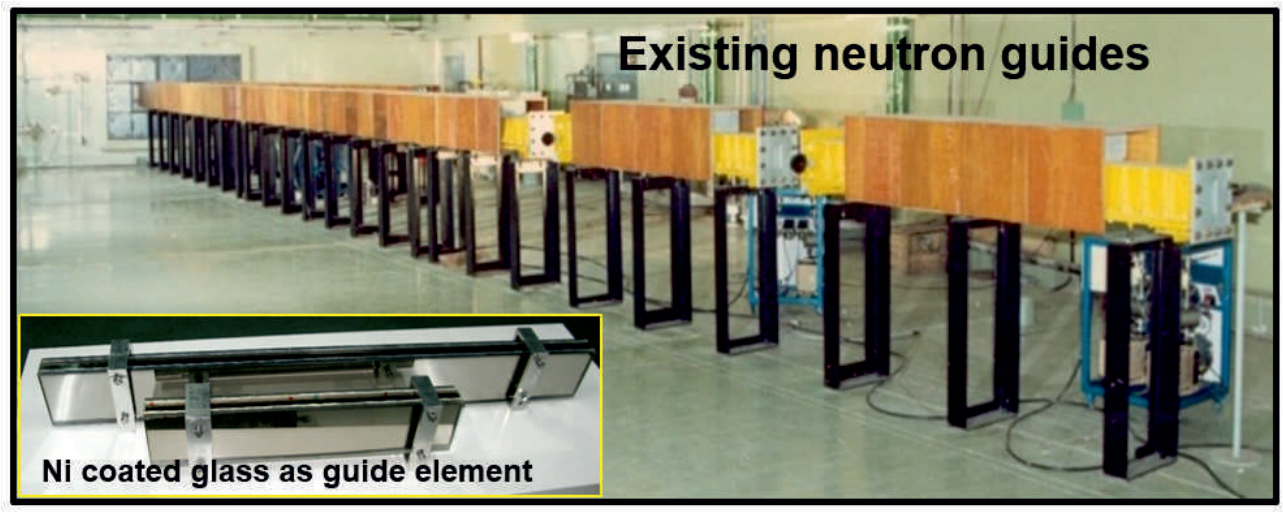

Indigenous development of new Ni/Ti (m=2) supermirror based neutron guides

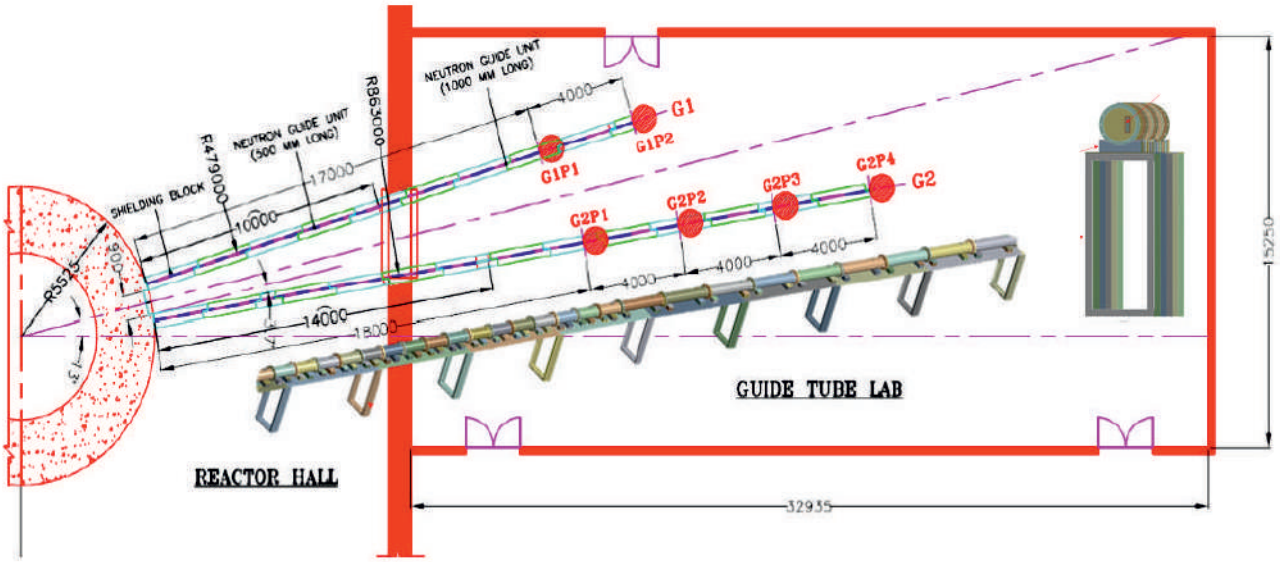

National Facility for Neutron Beam Research

Solid State Physics Division,
Bhabha Atomic Research Centre, Mumbai 400 085, India